HOKKAIDO UNIVERSITY

Title	LncRNA-dependent nuclear stress bodies promote intron retention through SR protein phosphorylation
Author(s)	Ninomiya, Kensuke; Adachi, Shungo; Natsume, Tohru et al.
Citation	EMBO Journal, 39(23), e102729 https://doi.org/10.15252/embj.2019102729
Issue Date	2020-02-03
Doc URL	https://hdl.handle.net/2115/79022
Rights	This is the peer reviewed version of the following article: The EMBO Journal: 39(3): e102729., which has been published in final form at https://doi.org/10.15252/embj.2019102729. This article may be used for non-commercial purposes in accordance with Wiley Terms and Conditions for Use of Self-Archived Versions.
Type	journal article
File Information	EMBOJ-2019-102729R1_Merged_PDF.pdf



Hokkaido University Collection of Scholarly and Academic Papers : HUSCAP

LncRNA-dependent nuclear stress bodies promote intron retention through SR protein phosphorylation

Kensuke Ninomiya[1], Shungo Adachi[2], Tohru Natsume[2], Junichi Iwakiri[3], Goro Terai[3], Kiyoshi Asai[3], and Tetsuro Hirose[1,4]

[1]Institute for Genetic Medicine, Hokkaido University, Sapporo 060-0815, Japan.

[2]Molecular Profiling Research Center, National Institute for Advanced Industrial Science and Technology (AIST), 135-0064, Koto-Ku, Tokyo, Japan.

[3]Graduate School of Frontier Sciences, University of Tokyo, Kashiwa, 277-8562, Japan.

[4]Corresponding author: Tetsuro Hirose, Institute for Genetic Medicine, Hokkaido University, Sapporo 060-0815, Japan. Phone: +81-11-70-6-5071, Fax +81-11-706-7540, e-mail: hirose@igm.hokudai.ac.jp

Running title: Function of nuclear stress bodies

Abstract

A number of long noncoding RNAs (lncRNAs) are induced in response to specific stresses to construct membrane-less nuclear bodies; however, their function remains poorly understood. Here, we report the role of nuclear stress bodies (nSBs) formed on highly repetitive satellite III (HSATIII) lncRNAs derived from primate-specific satellite III repeats upon thermal stress exposure. A transcriptomic analysis revealed that depletion of HSATIII lncRNAs, resulting in elimination of nSBs, promoted splicing of 533 retained introns during thermal stress recovery. A HSATIII-Comprehensive identification of RNA-binding proteins by mass spectrometry (ChIRP-MS) analysis identified multiple splicing factors in nSBs, including serine and arginine-rich pre-mRNA splicing factors (SRSFs), the phosphorylation states of which affect splicing patterns. SRSFs are rapidly dephosphorylated upon thermal stress exposure. During stress recovery, CDC like kinase 1 (CLK1) was recruited to nSBs and accelerated the re-phosphorylation of SRSF9, thereby promoting target intron retention. Our findings suggest that HSATIII-dependent nSBs serve as a conditional platform for phosphorylation of SRSFs by CLK1 to promote the rapid adaptation of gene expression through intron retention following thermal stress exposure.

Keywords: Noncoding RNA/nuclear stress bodies/intron retention/splicing factors/ phosphorylation

Introduction

Long noncoding RNAs (lncRNAs) have recently been recognized as fundamental regulators of gene expression, but their mechanisms of action remain largely unknown. Among the tens of thousands of human lncRNAs, a subset of architectural RNAs (arcRNAs) function as structural scaffolds of membrane-less subnuclear organelles or nuclear bodies (NBs) (Chujo, Yamazaki et al., 2016). NBs are usually located in inter-chromatin spaces in the highly organized nucleus and consist of specific factors that function in various nuclear processes (Banani, Lee et al., 2017). ArcRNAs sequestrate sets of specific RNA-binding proteins to initiate building of specific NBs near transcription sites (Chujo et al., 2016, Clemson, Hutchinson et al., 2009). Nuclear stress bodies (nSBs) were primarily reported 30 years ago (Mahl, Lutz et al., 1989) as primate-specific NBs that respond to thermal and chemical stresses. The assembly of nSBs is initiated alongside HSF1-dependent transcription of the primate-specific highly repetitive satellite III (HSATIII) lncRNA (Jolly, Usson et al., 1999) and heat shock-induced HSF1 aggregation (Jolly, Morimoto et al., 1997). HSATIII lncRNAs are transcribed from pericentromeric HSATIII repeated arrays on several human

chromosomes (Denegri, Moralli et al., 2002, Jolly, Konecny et al., 2002). These arrays are usually located in heterochromatinic regions that are transcriptionally silent; however, upon exposure to thermal stress, they are rapidly euchromatinized and produce HSATIII lncRNAs (Biamonti & Vourc'h, 2010). HSATIII lncRNAs are retained on chromosomes near their own transcription sites for several hours, even after stress removal, and recruit various RNA-binding proteins, including Scaffold attachment factor B (SAFB), HNRNPM, SRSF1, SRSF7, and SRSF9 (Denegri, Chiodi et al., 2001, Metz, Soret et al., 2004, Weighardt, Cobianchi et al., 1999), as well as specific chromatin-remodeling factors (Hussong, Kaehler et al., 2017, Kawaguchi, Tanigawa et al., 2015) and transcription factors (Jolly, Metz et al., 2004), which results in the assembly of nSBs.

SRSF1, SRSF7, and SRSF9 are serine and arginine-rich (SR) pre-mRNA splicing factors (SRSFs) that contain one or two RNA recognition motifs and a signature RS domain, an intrinsically disordered stretch of multiple SR (in part, SP or SK) dipeptides, near the C-terminus (Long & Caceres, 2009, Shepard & Hertel, 2009). The RS domain is required for protein-protein interactions with other SRSFs or RS domain-harboring proteins (Xiao & Manley, 1997). In addition, the functions of SRSFs in pre-mRNA splicing and mRNA export are modulated through phosphorylation of the RS domain

(Cao, Jamison et al., 1997, Graveley, 2000, Huang, Yario et al., 2004). Notably, the phosphorylation state of the RS domain is dynamically changed in response to environmental transitions, such as thermal stress or circadian changes in body temperature (Guil & Caceres, 2007, Preussner, Goldammer et al., 2017). Upon exposure to thermal stress, protein phosphatase 1 is activated to de-phosphorylate the RS domains of SR proteins, leading to modulation of a wide variety of pre-mRNA splicing events (Shi & Manley, 2007). Concomitantly, CDC2-like kinases 1 and 4 (CLK1 and CLK4), members of the nuclear SR protein kinase family, are induced upon thermal stress exposure to promote re-phosphorylation of SRSFs after stress removal (Ninomiya, Kataoka et al., 2011). These reports raise the intriguing possibility that nSBs are involved in the regulatory network of thermal stress-responsive pre-mRNA splicing by concentrating or sequestering SRSFs; however, the function of nSBs remains poorly investigated.

Here, we performed a genome-wide transcriptomic analysis of HeLa cells following knockdown of HSATIII lncRNAs to deplete nSBs, and found that HSATIII mainly promotes intron retention by hundreds of genes. Further investigation revealed that nSBs accelerate intron retention specifically during recovery from thermal stress. We also explored the protein composition of nSBs using chromatin isolation by

Comprehensive identification of RNA-binding proteins by mass spectrometry (ChIRP-MS) and an antisense oligonucleotide (ASO) of HSATIII lncRNA as a stable core component of nSBs. This analysis identified 141 proteins as putative nSB components in HeLa cells. Among them, we focused on CLK1, a SR protein kinase that is specifically recruited to nSBs during thermal recovery to re-phosphorylate SRSFs. Notably, we found that nSBs accelerate the rate of re-phosphorylation of SRSFs after stress removal. Phosphorylated SRSFs then promote retention of the HSATIII target introns. Based on our findings, we propose that nSBs serve as a platform to control the temperature-dependent phosphorylation states of selected SRSFs to regulate intron retention by hundreds of pre-mRNAs. The transcriptomic and subcellular proteomic analyses described here unveil the molecular events occurring in nSBs, which have remained enigmatic for the 30 years since their discovery.

Results

HSATIII lncRNAs facilitate intron retention in hundreds of mRNAs during stress recovery

To investigate the role of nSBs in stress-dependent gene expression, particularly splicing regulation, we analyzed global transcriptomic changes in HSATIII-depleted

HeLa cells (Figure 1A). Defective formation of two nSB subpopulations (Aly et al., 2019) was confirmed in HSATIII ASO-treated (HSATIII KD) cells exposed to thermal stress at 42°C for 2 h and recovery at 37°C for 1 h (Figure 1B and 1C). We confirmed that HSATIII depletion did not affect the integrity of other nuclear bodies such as nuclear speckles and paraspeckles (Figure EV1A~1E). Subsequently, RNA sequencing (RNA-seq) was used to compare the transcriptomes of control and HSATIII KD cells. To efficiently detect changes in splicing patterns, nuclear poly(A)+ RNAs were prepared from the isolated nuclei of control and HSATIII KD cells during the thermal stress recovery phase, and the expression levels of each annotated exon and intron were compared (Figure 1A). The expression levels of 533 introns in 434 genes and 3 exons in 3 genes were significantly decreased upon HSATIII knockdown (HSATIII KD/control<0.5) (Figure 1D and 1E). Changes in the expression levels of exons were hardly detectable, with a few exceptions (Figure 1E and EV1F). In addition, the expression levels of 17 introns in 17 genes and 4 exons in 4 genes were significantly increased upon HSATIII knockdown (HSATIII KD/control>2) (Figure 1C and 1D). For example, HSATIII knockdown reduced the expression levels of introns 2 and 3 of *TAF1D* (Figure 1F, blue bars), and decreased and increased the expression levels of intron 2 (blue bar) and exon 3 (red bar) of *DNAJB9*, respectively (Figure 1G).

Expression of the complete transcript of *DNAJB9* was increased in HSATIII KD cells, suggesting that nSBs may also affect expression through HSATIII independent mechanisms. These findings suggest that HSATIII lncRNAs mainly promote intron retention of pre-mRNAs during cell recovery from thermal stress.

We noticed that the sizes of the exons adjacent to HSATIII-targeted introns tended to be longer than the average size of exons (Figure 1H, see also Figure EV5F). To avoid sampling bias caused by the first and the last exons, which tend to be longer than internal exons, we compared the sizes of the exons adjacent to 399 HSATIII-targeted internal introns with those adjacent to 175,923 whole annotated human internal introns. Overall, 8.8% of the exons upstream and 10.3% of the exons downstream of HSATIII-targeted introns were longer than 1 kb (Figure 1H). By contrast, only 0.7% of exons adjacent to the whole annotated internal introns were longer than 1 kb, confirming that the exons adjacent to HSATIII-targeted introns tended to be longer than the average exon size.

A gene ontology analysis of 434 genes in which intron retention was promoted by HSATIII revealed a significant enrichment (FDR<0.05) of genes associated with multiple functions, including DNA/RNA metabolism, biosynthesis, stress response, and cell cycle (Table EV1). Only 57 and 30 of the 533 HSATIII-targeted introns were previously

identified as retained introns (also referred to as detained introns) in the human ENCODE database and a human glioblastoma cell line, respectively (Table EV2, discussed later) (Boutz, Bhutkar et al., 2015, Braun, Stanciu et al., 2017).

HSATIII lncRNAs promote intron retention during thermal stress recovery

To validate the RNA-seq data, we used CLK1 intron 3 and randomly selected 10 introns that were affected by HSATIII knockdown (10 down-regulated (fold change <-2) and 1 up-regulated (fold change >2); mean expression level>1e2) (Figure 1D) for quantitative RT-PCR (qRT-PCR) to analyze their levels in total RNAs from control and HSATIII KD cells. The levels of the intron-retaining pre-mRNAs were examined under three conditions: normal (37°C), thermal stress at 42°C for 2 h, and thermal stress at 42°C for 2 h followed by recovery at 37°C for 1 h (Figure 2A). For all down-regulated introns examined, the levels of intron retention were comparable in control and HSATIII KD cells during thermal stress, but were significantly lower in HSATIII KD cells than in control cells during the recovery phase (Figure 2A, upper panel). Notably, we recognized two distinct classes of intron retention during temperature transition: class 1 introns were retained at substantial levels under normal conditions, excised during thermal stress, and re-accumulated during stress recovery; and class 2 introns were

mostly excised under normal and thermal stress conditions, but retained during stress recovery (Figure 2A). Intron 1 of *PFKP* was an exceptional up-regulated intron that was retained during stress recovery of HSATIII KD cells (Figure 2A). A qRT-PCR analysis of subcellularly fractionated nuclear and cytoplasmic RNAs confirmed that all of the intron-retaining pre-mRNAs mentioned above were retained in the nucleus (Figure 2B), suggesting that mRNA export is prevented by the intron retention. In contrast to the marked effect on the levels of intron-retaining pre-mRNAs, HSATIII knockdown scarcely affected the levels of the cognate intron-removed (spliced) mRNAs. As exceptions, the levels of the spliced *DNAJB9*, *CLK1*, and *PFKP* mRNAs were significantly higher (*CLK1*, *DNAJB9*) or lower (*PFKP*) in HSATIII KD cells than in control cells (Figure 2A, lower panel).

Next, the levels of the intron-retaining pre-mRNAs and the spliced mRNAs were measured in newly synthesized nascent RNA pools captured by pulse-labeled RNAs with ethinyl uridine (see Figure 2C and STAR methods). As shown in Figure 2D and 2E, with the exception of *PFKP*, the levels of the intron-retaining pre-mRNAs were lower in HSATIII KD cells than in control cells. By contrast, with the exceptions of *EP400* and *PFKP*, the levels of the spliced mRNAs were significantly higher in HSATIII KD cells than in control cells. Overall, these data suggest that HSATIII promotes intron retention

by suppressing splicing of newly synthesized transcripts.

HSATIII affects the kinetics of accumulation of intron-retaining pre-mRNAs during thermal recovery

Among the retained introns regulated by HSATIII, a subpopulation of the *CLK1* mRNA reportedly localizes in the nucleus as a partially unspliced pre-mRNA that retains introns 3 and 4 (Figure 3A) (Duncan, Howell et al., 1995, Ninomiya et al., 2011). Excision of retained introns is induced by thermal and osmotic stresses, neuronal activity, and inhibition of CLK1 kinase activity to produce mature mRNAs (Mauger, Lemoine et al., 2016, Ninomiya et al., 2011). We also detected another spliced isoform of the *CLK1* mRNA produced by skipping of exon 4, which is committed to nonsense-mediated mRNA decay (Figure 3A). Consequently, we examined the effect of HSATIII knockdown on thermal stress-responsive excision of the retained introns of the *CLK1* pre-mRNA at several time points using semi-quantitative RT-PCR. As reported previously (Ninomiya et al., 2011), the retained introns were excised to form the mature mRNA in both control and HSATIII KD cells after a 2 h thermal stress exposure (Figure 3B, 42°C, 2 h). In control cells, the level of the intron 3 and 4-retaining *CLK1* pre-mRNA was restored within 1 h after stress removal (Figure 3B, lanes 6–10, and Figure 3C).

Notably, this process was markedly delayed in HSATIII KD cells, in which restoration of the original level of the intron 3 and 4-retaining *CLK1* pre-mRNA took longer than 4 h (Figure 3B, lanes 1–5, and Figure 3C).

Like *CLK1*, *TAF1D* has two HSATIII target introns (Figure 1E) that border a cassette-type exon 3 (Figure EV2A). Semi-quantitative RT-PCR confirmed that the partially unspliced *TAF1D* pre-mRNA retaining introns 2 and 3 underwent splicing upon thermal stress and was rapidly re-accumulated after stress removal in control cells (Figure EV2B). However, this re-accumulation was markedly delayed in HSATIII KD cells (Figure EV2B). In addition, we also examined the levels of the *DNAJB9* mRNA, another intron-retaining RNA that harbors a single HSATIII target intron (Figure EV2A), and found that intron retention was detectable in control cells but not HSATIII KD cells (Figure EV2B). We also confirmed that the thermal stress-responsive alternative splicing of the *HSP105* and *TNRC6a* mRNAs reported previously (Yamamoto, Furukawa et al., 2016, Yasuda, Nakai et al., 1995) was barely affected by HSATIII knockdown (Figure EV2C), indicating selectivity of target pre-mRNAs by HSATIII lncRNAs.

To further support the proposal that HSATIII lncRNAs promote intron retention, we used a gain-of-function approach using a somatic hybrid Chinese hamster ovary (CHO)

cell line possessing human chromosome 9 (CHO (His9)) (Tanabe, Nakagawa et al., 2000). Since HSATIII is primate-specific, these lncRNAs are only expressed from human chromosome 9 in CHO (His9) cells upon thermal stress, and form nSB-like granules with hamster SRSF1 (Figure 3D and 3E). A time course analysis of the splicing pattern of the endogenous hamster *Clk1* mRNA revealed that re-accumulation of the intron-retaining pre-mRNA after stress removal was markedly faster in CHO (His9) cells than in control CHO cells (Figure 3F and 3G). Notably, HSATIII knockdown abolished the acceleration effect in CHO (His9) cells (Figure 3H). Taken together, these data suggest that HSATIII lncRNAs are required and sufficient for acceleration of intron retention of the *CLK1* pre-mRNA during stress recovery, and this process was likely acquired in primate species.

Multiple SRSFs and SR-related proteins interact with HSATIII in nSBs

To examine the molecular mechanism of intron retention by HSATIII lncRNAs, we attempted to comprehensively identify the proteins associated with HSATIII, which likely correspond to nSB components. ChIRP was employed to pull down the ribonucleoprotein (RNP) complexes of HSATIII using a biotinylated ASO (Figure 4A). Because HSATIII lncRNAs consist of multiple GGAAU repetitive sequences (Jarmuz,

Glotzbach et al., 2007, Valgardsdottir, Chiodi et al., 2005), HSATIII RNP complexes could be efficiently captured by a single biotinylated HSATIII ASO consisting of four tandem repeats of ATTCC. ChIRP was carried out using formaldehyde-crosslinked HeLa cells that were treated at 42°C for 2 h followed by recovery at 37°C for 1 h. A RT-PCR analysis revealed efficient (>10%) and specific precipitation of HSATIII with the HSATIII ASO from thermally stressed cells (Figure 4B). As a negative control, neither the NEAT1 nuclear lncRNA nor the *GAPDH* mRNA was precipitated with the HSATIII ASO (Figure 4B). Silver staining of the coprecipitated proteins in a SDS-PAGE gel identified multiple bands that were strongly detected in the stressed cells, but were only detected as faint background signals in the control samples (Figure 4C). A liquid chromatography mass spectrometry analysis revealed that 141 proteins, most of which that have not yet been reported as nSB components, were specifically coprecipitated with HSATIII lncRNAs from the stressed cells (Table EV3). Most of these proteins are likely RNA-binding proteins that possess canonical RNA-binding domains. A gene ontology analysis revealed significant enrichment of proteins functionally associated with nuclear RNA processing, such as pre-mRNA splicing, 3'-end processing, and export of mRNAs (Table 1). Notably, most SRSFs and HNRNPs, including known nSB components (SAFB, SRSF1, SRSF7, SRSF9, and HNRNPM), were identified as major

components. In addition to SRSFs, non-classical SR proteins and RNA-binding SR-related proteins, which harbor one or more clusters of SR and SP dipeptides, such as TRA2A, TRA2B, U2AF35, U2AF65, LUC7L, SRRM1, BCLAF1, THRAP3, and PPHLN1 (Castello, Fischer et al., 2012, Long & Caceres, 2009), were also identified (Table EV3). Although the number of peptides was limited, the CLK1 SR protein kinase was detected in the ChIRP fraction (described below). By contrast, some previously reported nSB-localized proteins, such as HSF1, CBP, SWI/SNF components, and BRD4, were undetectable in our ChIRP-MS analysis (Table EV3). The nSB localization of the proteins identified above was confirmed by western blotting of the ChIRPed proteins (Figure 4D) and/or immunofluorescence (Figure 4E). The SR-related TRA2B and THRAP3 proteins interacted and colocalized with HSATIII in nSBs (Figure 4D, 4E and 4F). The transiently expressed PPHLN1 protein was also colocalized with HSATIII in nSBs (Figure 4G). These results indicate that SR-related proteins, as well as SRSFs, selectively interact with HSATIII in nSBs.

CLK1 is recruited to nSBs during thermal stress recovery

As described above, CLK1 was detected in the HSATIII-ChIRP fraction (Table EV3). CLK1 is a nuclear SR protein kinase that phosphorylates and modulates the

activity of SRSFs in pre-mRNA splicing (Duncan, Stojdl et al., 1997), raising the intriguing possibility that phosphorylation of SRSFs in nSBs is modulated by CLK1. Consequently, we monitored its interaction with HSATIII by ChIRP at five time points during temperature transitions from 37°C to 42°C for 1, 2, or 3 h, or 37°C to 42°C for 2 h followed by recovery at 37°C for 1 h. CLK1 was specifically coprecipitated with HSATIII following recovery after 2 h exposure to thermal stress (Figure 5A). By contrast, CLK1 was poorly detected after thermal stress for 2 or 3 h without recovery at 37°C (Figure 5A), suggesting that the temperature shift from 42°C to 37°C is required to recruit CLK1 onto HSATIII. The nSB components SRSF7 and SRSF9 interacted with HSATIII after a 2 h exposure to thermal stress alone (Figure 5A), suggesting that, unlike CLK1, they do not require the subsequent temperature shift to 37°C for this interaction.

Next, we examined the localization of CLK1 in HeLa cells following thermal stress at 42°C for 2 h and recovery at 37°C for 1 h. We confirmed that transiently expressed FLAG-CLK1 and its kinase-dead mutant (CLK1KR) mimicked the behavior of endogenous CLK1 (Figure 5B and 5C). FLAG-CLK1WT and KR were poorly detectable in nSBs after exposure to thermal stress for 2 h, but relocated to nSBs after recovery at 37°C (Figure 5D, 5E, EV3A and EV3C). These data indicate that the nSB localization of CLK1 occurs during stress recovery and correlates with the interaction with HSATIII

lncRNAs. Since FLAG-CLK1 is reported to result in partially diffuse nuclear speckles (Colwill, Pawson et al., 1996), FLAG-CLK1KR, which did not affect the integrity of nuclear speckles, was used to monitor the localization of CLK1 in nuclear speckles. Iimmunofluorescence analysis revealed that FLAG-CLK1KR predominantly localized to nuclear speckles with SRSF2 under normal conditions (Figure EV3B and EV3D).

To obtain mechanistic insights into the temperature-dependent recruitment of CLK1 to nSBs, we used HSATIII-ChIRP to examine the interaction of CLK1 truncated mutants with nSBs during stress recovery (Figure 5B). CLK1 interacts with substrate proteins such as SRSFs and homo-dimerizes via its N-terminal intrinsically disordered region (IDR) (Duncan et al., 1995, Keshwani, Hailey et al., 2015). In addition, the C-terminal kinase domain phosphorylates the substrates (Bullock, Das et al., 2009). The C-terminal truncated CLK1 mutant (FLAG-CLK1ΔC in Figure 5B) localized to nuclear speckles at 37°C but not upon thermal stress, and relocalized to nSBs after stress removal (Figure EV3E-3H). The CLK1ΔN mutant possessed a SV40 nuclear localization signal instead of the original NLS present in the deleted N-terminal domain and was properly imported into the nucleus (Figure EV3I). CLK1ΔC was coprecipitated with HSATIII much more efficiently under the stress recovery condition than under the thermal stress condition, whereas CLK1ΔN was poorly precipitated under any condition

(Figure 5F), indicating that the N-terminal domain of CLK1 is necessary and sufficient for its temperature-dependent interaction with HSATIII. We also examined whether SRSFs anchor CLK1 to nSBs. SiRNA-mediated knockdown of SRSF9, one of the major nSB-localized SRSFs, resulted in a significant reduction in the interaction of FLAG-CLK1WT or CLK1ΔC with HSATIII (Figure 5G and 5H), indicating that SRSF9 contributes to the recruitment of CLK1 at nSBs.

The amino acid sequences of the C-terminal kinase domains of CLK family proteins (CLK1–4) are highly conserved. By contrast, the N-terminal IDRs are similar in CLK1 and CLK4, but are only partly conserved between CLK1/4 and CLK2. Consequently, we examined the involvement of the N-terminal IDRs of ubiquitously expressed CLK2 and CLK4 in nSB recruitment. The N-terminal IDRs of CLK2 and CLK4 were coprecipitated with HSATIII by ChIRP and colocalized with HSATIII after 1 h thermal stress recovery (Figure EV3J and EV3K), indicating that both proteins are able to relocate to nSBs during stress recovery through their poorly conserved N-terminal IDRs.

nSBs are platforms for the rapid re-phosphorylation of SRSFs by CLK1 during thermal recovery

Next, we examined the subnuclear localization of CLK1 and SRSFs during thermal stress and recovery. First, we confirmed that SRSF9 colocalized with HSATIII in nSBs after 2 h thermal stress exposure and after stress removal (Figure 6A), which is consistent with the ChIRP results (Figure 5A). We also confirmed that the SRSF9 foci were diminished and diffused throughout the nucleoplasm in HSATIII KD cells (Figure EV4A). Moreover, we confirmed colocalization of CLK1 and SRSF9 in nSBs during stress recovery (Figure 6B and 6C). Conversely, SRSF9 was poorly detectable in nuclear speckles marked by SRSF2, which are distinct from nSBs (Figure EV4B~4D). SRSFs are rapidly de-phosphorylated upon thermal stress (Shi & Manley, 2007); therefore, it is possible that CLK1 is recruited to nSBs during stress recovery to promote re-phosphorylation of SRSFs. To analyze the phosphorylation states of SRSFs after thermal stress and recovery, we examined SRSF9, which possesses a short RS domain with four SRs and three SPs. Western blotting followed by Phos-tag SDS-PAGE (Kinoshita, Kinoshita-Kikuta et al., 2008) revealed multiple bands corresponding to different phosphorylation states of SRSF9 (Figure 6D and 6F). Under normal conditions (37°C), five discrete SRSF9 bands were detected (Figure 6F, lane 1). After thermal stress at 42°C for 2 h (Figure 6F, lane 3), two fast migrating bands (likely hypo-phosphorylated SRSF9) appeared and the upper bands (likely

hyper-phosphorylated SRSF9) were diminished (Figure 6F, indicated by arrowheads and arrows, respectively). After recovery at 37°C for 1 h, the band pattern was mostly restored to its original state (Figure 6F, lane 4); however, this restoration was abolished by administration of the CLK1 inhibitor KH-CB19 (Fedorov, Huber et al., 2011) at the beginning of the stress recovery phase (Figure 6D and 6F, lane 5). These findings suggest that the observed band shift to lower positions after heat stress and subsequent restoration after stress removal were caused by thermal stress-induced de-phosphorylation and CLK1-dependent re-phosphorylation of SRSF9, respectively. To determine whether nSBs affect CLK1-dependent re-phosphorylation of SRSF9, we examined the Phos-tag band pattern of SRSF9 in HSATIII KD and control cells (Figure 6E, also see EV4J). Restoration of the band pattern of SRSF9 after stress removal was markedly delayed in HSATIII KD cells (Figure 6F, right). The hyper-phosphorylated band (Figure 6F and 6G, arrow a) was mostly restored after 1 h recovery in control cells, but this restoration was delayed until 4 h after stress removal in HSATIII KD cells. In addition, the hypo-phosphorylated bands (Figure 6F and 6G, arrowheads c and d) were rapidly diminished after 1 h recovery in control cells but this process was delayed in HSATIII KD cells. Similar HSATIII-dependent restoration of the band pattern of SRSF1 was observed after stress removal (Figure EV4E). Western blotting of phosphorylated

SRSFs using pan-phospho SR antibody (1H4), which mainly detects SRSFs possessing a longer RS domain (such as SRSF4, 5, 6 and 10), revealed that thermal stress inducible dephosphorylation and subsequent rephosphorylation of SRSFs during stress recovery occurred with slower kinetics which were not affected by depletion of HSATIII (Figure EV4F), suggesting that HSATIII is specifically involved in the rapid rephosphorylation of SRSF9 during stress recovery.

To confirm that CLK1-dependent re-phosphorylation of SRSF9 occurs within nSBs, we performed Phos-tag western blotting followed by HSATIII-ChIRP analyses of HeLa cells exposed to control conditions (37°C), 42°C for 2 h, or 42°C for 2 h followed by recovery for 1 h at 37°C (Figure 6H and 6I, also see Figure EV4G). In the HSATIII-ChIRP fractions, de-phosphorylated SRSF9 (the lower band marked by arrowhead d) was diminished and phosphorylated SRSF9 (marked by arrow a) was markedly increased during the 1 h recovery (Figure 6H, lanes 2, 4, 6, and 8, and Figure 6I). Notably, these changes were inhibited in the presence of KH-CB19 (Figure 6H, lane 8 and Figure 6I). Western blot analyses of the HSATIII-ChIRP samples revealed that the amount of coprecipitated SRSF9 did not change markedly during the 1 h recovery, regardless of the presence or absence of KH-CB19 (Figure EV4H). Taken together, these data suggest that CLK1 recruited during stress recovery re-phosphorylates

SRSF9 within nSBs. Although differentially phosphorylated bands were not clearly separated on the Phos-tag gel, stress-induced mobility shifts of nSB-localized SRSF1, which likely correspond to the hypophosphorylated form (Figure EV4J), were restored after stress removal in a CLK1-dependent manner (Figure EV4I and EV4J), suggesting that CLK1 rapidly re-phosphorylates various SRSFs in nSBs during stress recovery.

CLK1-dependent phosphorylation of SRSF9 in nSBs underlies the promotion of intron retention during stress recovery

The findings described above raised the intriguing possibility that recruitment of CLK1 to nSBs for rapid re-phosphorylation of SRSFs promotes intron retention of mRNAs during thermal stress recovery. To address this possibility, we investigated the effect of SRSF knockdown on intron retention. Depletion of SRSF1 remarkably disrupted nSBs (Figure EV5A-EV5C), such that we were unable to investigate the effect of SRSF1 on nSB-dependent splicing regulation. Consequently, we investigated the effect of SRSF9 knockdown on intron retention of HSATIII target mRNAs using newly synthesized nascent RNA pools (Figure 7A). With the exception of *PFKP*, SRSF9 knockdown reduced the levels of the intron-retaining mRNAs (Figure 7A) and increased the levels of the spliced forms of the mRNAs (Figure 7B). These results suggest that

SRSF9 suppresses pre-mRNA splicing to promote HSATIII-dependent intron retention. RT-PCR analyses revealed that SRSF9 depletion diminished the prominent accumulation of the *CLK1* and *TAF1D* mRNAs retaining two sequential introns after 1 h recovery from thermal stress (Figure 7C and 7D). Consistently, publicly available eCLIP data showed that multiple eCLIP tags of SRSF9 mapped to the exons adjacent to the retained introns of the *CLK1* and *TAF1D* mRNAs in HepG2 cells (Figure EV4C).

Next, we examined the possibility that CLK1-dependent re-phosphorylation of SRSF9 in nSBs is responsible for the regulation of intron retention. To investigate its requirement for the changes in intron retention after stress removal, CLK1 kinase activity was impeded by KH-CB19 during thermal stress recovery (Figure 7E and 7F). HSATIII-dependent intron retention (and the opposite effect on the *PFKP* mRNA) was impaired in the presence of KH-CB19 (*EP400* was an exception), which supports our hypothesis that CLK1-dependent re-phosphorylation of SRSFs is required for the promotion of intron retention. To directly investigate the role of phosphorylation of SRSF9 in splicing regulation, we compared the effects of wild-type SRSF9 (SRSF9-WT) and its de-phosphorylated mutant (SRSF9-mut), in which all SP and SR dipeptides were replaced by AP and AR, respectively (Figure 7G and Figure EV4D), on splicing of the *TAF1D* and *DNAJB9* splicing reporter minigenes. Western blot analyses of a Phos-tag

gel detected multiple FLAG-SRSF9-WT protein bands that shifted to lower hypo- or de-phosphorylated bands after thermal stress (Figure 7G). By contrast, the SRSF9-mut was detected as a single band with the same mobility as the thermal stress-induced de-phosphorylated WT protein, even at 37°C (Figure 7G, arrowhead), and was no longer shifted by thermal stress (Figure 7G), indicating that the SRSF9-mut mimics de-phosphorylated SRSF9.

To replace endogenous SRSF9 with FLAG-SRSF9-WT or the de-phosphorylated mutant, HeLa cells were co-transfected with SRSF9 siRNA and siRNA-resistant FLAG-SRSF9 expression plasmids (Figure EV5F). These cells were also transfected with splicing reporter *TAF1D* and *DNAJB9* plasmids, and the splicing patterns were examined after exposure to thermal stress for 2 h followed by recovery for 1 h (Figure 7H and 7I). SRSF9-WT suppressed splicing of the reporter RNAs, whereas SRSF9-mut did not, suggesting that phosphorylation of the RS domain of SRSF9 is required to promote intron retention of the *TAF1D* and *DNAJB9* mRNAs by suppressing splicing. Taken together, these findings suggest that the re-phosphorylation of the RS domain of SRSF9 by CLK1 in nSBs promotes intron retention of target mRNAs during thermal stress recovery.

Discussion

In this study, next-generation sequencing-based screening of the regulatory targets of nSBs identified a major molecular function of nSBs in promoting intron retention by more than 400 mRNAs during thermal stress recovery. In recent years, a number of studies have examined conditional intron retention in the nucleus and its biological functions, such as regulation of stress responses, the cell cycle, neuronal activity, learning and memory, spermiogenesis, and tumor growth (Boutz et al., 2015, Braun et al., 2017, Dominguez, Tsai et al., 2016, Gill, Park et al., 2017, Mauger et al., 2016, Naro, Jolly et al., 2017). Thus, nuclear intron retention is being accepted as a regulatory mechanism that fine tunes gene expression under various biological conditions. Here, we found that nSBs assembling around HSATIII arcRNA scaffolds are novel molecular machineries that regulate nuclear intron retention during thermal stress recovery. Comparison of the 533 retained HSATIII-targeted introns identified here with the 3968 retained introns previously reported in the U87 human glioblastoma cell line revealed an overlap of only 30 introns (Table EV2). It is possible that different introns are selected for retention under different physiological conditions, presumably through the use of distinct regulatory factors.

We confirmed that SRSF9 promotes intron retention of HSATIII-targeted

pre-mRNAs (Figure 7A). SRSFs are generally considered to promote splicing in a phosphorylation-dependent manner; however, SRSF9 is a repressor of 3' splice site utilization (Simard & Chabot, 2002). In this case, SRSF9 suppresses splicing by recognizing a specific intronic CE9 element; however, no sequence motif similar to CE9 was found in the HSATIII-dependent retained introns that we identified. According to the public eCLIP database, multiple peaks of SRSF9 eCLIP tags were detectable in the HSATIII-targeted retained introns, as well as adjacent upstream and downstream exons; however, no significant enrichment of SRSF9 eCLIP tags compared with the average numbers in general introns and exons was detected (Figure EV5G), suggesting that SRSF9 is required but not sufficient for HSATIII-dependent intron retention. The effect of SRSF9 knockdown was weaker than the effect of HSATIII knockdown, raising the possibility that SRSF9 functions redundantly with other nSB-localized SRSFs. Detection of eCLIP tags of SRSF1 and SRSF7 near the positions of the SRSF9 eCLIP tag may support this possibility (Figure EV5D).

Consistent with previous reports (Boutz et al., 2015, Ninomiya et al., 2011), we found that the catalytic activity of CLK1 is required for HSATIII-dependent intron retention. We also found that CLK1 phosphorylates SRSF9 during thermal stress recovery; this phosphorylation was detected in the HSATIII-ChIRP fraction, suggesting

that it occurs within nSBs. Furthermore, the results of a splicing reporter assay using model constructs for intron retention support the proposal that CLK1-dependent phosphorylation of the serine residues of SR/SP repeats in SRSF9 promotes intron retention (Figure 7G–I). Among the tested introns, the retention of *PFKP* intron 1 was exceptionally down-regulated by HSATIII, SRSF9, and the catalytic activity of CLK1, suggesting that a common molecular mechanism can have opposing effects on a minor population of target introns. Intron retention of *EP400* moderately required SRSF9 but not CLK1 activity (Figure 7A and 7F), suggesting the existence of a CLK1-independent mechanism to promote intron retention. We propose a model of nSB function (Figure 7J) in which SRSFs are globally de-phosphorylated upon thermal stress at 42°C (Shin, Feng et al., 2004), and HSATIII arcRNAs are simultaneously synthesized to form nSBs that sequestrate subsets of de-phosphorylated SRSFs. Under this condition, the retention of class 1 introns is suppressed to produce mature mRNAs. Following recovery to normal conditions (37°C), CLK1 is recruited to nSBs, where it re-phosphorylates the sequestrated SRSFs, which then act to rapidly promote retention of class 1 and 2 introns within 1 h (Figure 7J). These intron retention events may occur outside of nSBs since the intron-retaining pre-mRNAs were barely detected in the HSATIII-ChIRP fraction. Therefore, the re-phosphorylated SRSFs likely relocate from

nSBs to the nucleoplasm, which is analogous to the mechanism of mobilization of SRSFs from nuclear speckles to the nucleoplasm through phosphorylation by CLK1 (Colwill et al., 1996). Consequently, we argue that nSBs act as a platform for phosphorylation of sequestrated SRSFs by CLK1 to promote intron retention during thermal stress recovery.

Recruitment of CLK1 to nSBs in response to a temperature change from 42°C to 37°C is considered a critical step for rapid re-phosphorylation of SRSFs within nSBs. This temperature-sensitive recruitment of CLK1 requires its N-terminal IDR. CLK family kinases commonly contain long flexible N-terminal IDRs that resemble the RS domains of SRSFs. The N-terminal IDR of CLK1 contacts both the kinase domain and the RS domain of SRSF1 to induce hyper-phosphorylation of SRSF1 (Aubol, Plocinik et al., 2014). We observed that recruitment of CLK1 to nSBs requires the presence of SRSF9, suggesting that the analogous interaction between the CLK1 N-terminal IDR and SRSF9 is responsible for recruitment of CLK1 to nSBs. The mechanism by which the CLK1 N-terminal IDR senses the temperature change remains elusive. It is possible that thermal stress induces a structural change in the N-terminal IDR of CLK1 that interferes with its contact with the RS domains of SRSF9. The N-terminal IDRs of CLK2 and CLK4 also associate with nSBs in a similar temperature-sensitive manner, suggesting that

other CLK family kinases contribute to the phosphorylation of SRSFs in nSBs. The amino acid sequences of the N-terminal IDRs are poorly conserved among CLK family kinases, suggesting that short stretches and/or the compositional property of amino acids among the IDRs might be responsible for the temperature-sensitive recruitment of CLKs to nSBs. CLKs are localized in nuclear speckles at normal temperatures, where they phosphorylate SRSFs and SR-related proteins (Colwill et al., 1996, Gui, Lane et al., 1994). The localization of CLK1 to nuclear speckles is maintained under thermal stress, suggesting that the mechanism used to localize CLK1 to nSBs differs from that used for nuclear speckle localization. This variation may be due to the different compositions of SRSFs in nSBs and nuclear speckles and might ensure selective and rapid phosphorylation of specific classes of SRSFs during stress recovery.

In addition to classical SRSFs, we identified other SR-related proteins, including TRA2B and BCLAF1/THRAP3, that also have SR/SP dipeptides as potential sites of phosphorylation by CLKs (Aubol, Plocinik et al., 2013). These SR-related proteins reportedly form a complex with SRSF1, SRSF9, SAFB, and CLKs (Nayler, Stratling et al., 1998, Tai, Geisterfer et al., 2003), raising the possibility that multiple SR and SR-related proteins interact through the IDRs to form the massive membrane-less structure of nSBs, where they are collectively re-phosphorylated by CLKs. The effect of

HSATIII on the intron retention of *CLK1* and *TAF1D* pre-mRNAs was limited to within 4 h after stress removal (Figure 3B, 3C, and Figure EV1B). This time course of intron retention correlates with that of SRSF9 re-phosphorylation (Figure 6F). It is likely that nSBs function to rapidly restore the proper levels of intron-retaining pre-mRNA in the nucleus during stress recovery. nSBs also affect the level of at least a few spliced mature mRNAs through intron retention (Figure 2A), indicating that they may alter the levels of their translation products. In addition to the role of intron retention as a regulatory mechanism for fine tuning gene expression, it was recently reported that a subset of introns act as ncRNAs that trap the spliceosome and decrease global splicing upon nutrient depletion in yeast (Morgan, Fink et al., 2019, Parenteau, Maignon et al., 2019). In addition, a role of introns in prevention of R-loop and DNA damage accumulation has also been reported (Bonnet, Grosso et al., 2017). Further investigations will reveal the biological significance of HSATIII-dependent intron retention to cellular and physiological events. Multiple proteins associated with other RNA processing events, including 3'-end processing, nuclear export, stability control, and modification of mRNAs (Table 1 and Table EV3), are found in nSBs, suggesting the involvement of nSBs in controlling mRNA processing events other than splicing during thermal stress and recovery. Further elucidation of the cellular and physiological roles of

HSATIII-dependent nSBs will give important clues to understand the significance of the satellite repeat expansion that specifically occurs in primate genomes.

Materials and Methods

Cell culture

HeLa cells were cultured in Dulbecco's modified Eagle's medium (DMEM) (Nacalai Tesque) supplemented with antibiotics (100 U/ml streptomycin and 100 μg/ml penicillin; Sigma) and 10% fetal calf serum (Sigma) at 37°C in 5% CO_2. CHO cells were cultured in DMEM/Ham's F-12 medium (Nacalai Tesque). CHO (His9) cells (JCRB Cell Bank) were grown in medium containing 10 mM L-histidinol (Sigma) to maintain human chromosome 9, and cultured in normal medium from the day before the analysis. For thermal stress induction, the cells were incubated at 42°C in an incubator with 5% CO_2.

Plasmid construction

To construct plasmids expressing FLAG-tagged full-length and partial proteins, each DNA fragment was amplified from human cDNA by PCR and introduced in-frame into the pcDNA5/FRT/TO-FLAG vector. The FLAG-SRSF9 expression plasmid (pcDNA3-FLAG-SRSF9) was kindly provided by Dr. Kataoka (Univ. Tokyo). Inverted PCR-based mutagenesis was used to construct plasmids expressing the CLK1 KR

mutant or the SRSF9 mutant and its siRNA-resistant mutants. To construct the splicing reporter plasmids, *TAF1D* and *DNAJB9* intron-containing DNA fragments were amplified by PCR from human genomic DNA and introduced in-frame into the pEGFP-C1 vector.

ChIRP

ChIRP was performed as described previously (Chu, Quinn et al., 2012). Cultured cells at 80–90% confluence (one or two 10 cm culture dishes for each sample) were immediately crosslinked in 10 ml of 1% paraformaldehyde (PFA)/PBS per 10 cm dish for 15 min at room temperature, and the crosslinking reaction was stopped by adding 1 ml of 1.5 M glycine. The crosslinked cells were then washed with 10 ml of ice-cold PBS twice, suspended in 1 ml of ice-cold PBS using a scraper, and collected in microtubes by microcentrifugation. After removing the PBS, the cells were resuspended in 350 μl of lysis buffer (50 mM Tris-Cl pH 7.0, 10 mM EDTA, 1% SDS, 1 mM PMSF, cOmplete™ Protease Inhibitor Cocktail (Sigma), and RNAse inhibitor (Thermo Fisher Scientific)) and disrupted using a Bioruptor (Cosmo Bio) (15 sec ON, 45 sec OFF, 118 cycles). Subsequently, the insoluble fraction was removed by microcentrifugation for 10 min at 15°C, and the supernatant was used for ChIRP. Two volumes of hybridization buffer (750 mM NaCl, 1% SDS, 50 mM Tris-Cl pH 7.0, 1 mM EDTA, 15% (v/v) formamide, 1

mM PMSF, cOmplete™ Protease Inhibitor Cocktail (Sigma), and RNAse inhibitor) and the HSATIII antisense or control oligonucleotide were added. The mixture was incubated at 37°C for 4 h, mixed with Dynabeads MyOne Streptavidin C1 (Thermo Fisher Scientific), and incubated for 30 min. The beads were then washed five times for 5 min at 37°C with 0.8 ml of wash buffer (2× SSC and 0.5% SDS). The bound proteins were eluted and reverse-crosslinked by boiling in SDS sample buffer (95°C for 30 min). For mass spectrometry, the bound proteins were eluted with 100 mM Tris-HCl (pH 8.0) and 2% SDS. For silver staining, the eluted proteins were separated by SDS-PAGE and stained using the SilverQuest Silver Staining Kit (Thermo Fisher Scientific) according to the manufacturer's manual. For Phos-tag western blotting of ChIRP samples, the eluate and input proteins were collected by trichloroacetic acid precipitation and resuspended in new SDS sample buffer. The bound RNAs were eluted by protease K treatment (50°C for 45 min) followed by heating (95°C for 10 min) and purification as described below.

Mass spectrometry

To remove the SDS from eluted samples, the methanol-chloroform protein precipitation method was used. Briefly, four volumes of methanol, one volume of chloroform, and three volumes of water were added to the eluted sample and mixed

thoroughly. The samples were centrifuged at 20,000 g for 10 min, the water phase was carefully removed, four volumes of methanol were added, and the samples were centrifuged at 15,000 rpm for 10 min. Subsequently, the supernatant was removed and the pellet was washed once with 100% ice-cold acetone. The precipitated proteins were re-dissolved in guanidine hydrochloride, reduced with Tris(2-carboxyethyl)phosphine hydrochloride, alkylated with iodoacetamide, and then digested with lysyl endopeptidase and trypsin. The peptide mixture was applied to a Mightysil-PR-18 (Kanto Chemical) frit-less column (45 x 0.150 mm ID) and separated using a 0–40% gradient of acetonitrile containing 0.1% formic acid for 80 min at a flow rate of 100 nL/min. The eluted peptides were sprayed directly into a mass spectrometer (Triple TOF 5600+; AB Sciex). MS and MS/MS spectra were obtained using the information-dependent mode. Up to 25 precursor ions above an intensity threshold of 50 counts/s were selected for MS/MS analyses from each survey scan. All MS/MS spectra were searched against protein sequences of the RefSeq (NCBI) human protein database (RDB) using the Protein Pilot software package (AB Sciex), and decoy sequences were then selected with a false discovery rate <1%.

Nucleus/cytoplasm fractionation

Nucleus/cytoplasm fractionation was performed as described previously (Mili, Shu et al., 2001), with minor modifications. Cultured cells on a 35 mm dish were suspended in 200 μl of RSB-100 (10 mM Tris-HCl pH 7.4, 100 mM NaCl, and 2.5 mM $MgCl_2$) containing 40 μg/ml digitonin, and centrifuged at 2,000 g for 2 min at 4°C. The supernatant was collected as the cytoplasmic fraction. The pellet (nuclear fraction) was resuspended in 200 μl of RSB-100 buffer. The fractions were lysed in 600 μl of TRI Reagent LS for RNA analysis or 200 μl of 2× SDS sample buffer (200 mM dithiothreitol, 100 mM Tris-HCl pH 6.8, 4% SDS, and 20% glycerol) for western blot analysis.

Transfection and knockdown

For transfection followed by cell staining or ChIRP, plasmids were transfected into cells using TransIT-LT1 reagent (Mirus) 16–18 h before the assay (0.2 μg of plasmid, 100 μl of opti-MEM, and 1 μl of TransIT reagent were used per 1 ml of culture medium). For siRNA knockdown, Stealth siRNA (Thermo Fisher Scientific) was transfected at a final concentration of 10 nM using Lipofectamine RNAiMAX (Thermo Fisher Scientific) 48 h before the experiments. For the splicing reporter assay, the cells were transfected using 12 pmol of Stealth siRNA, 50 ng of splicing reporter plasmid, 300 ng of SRSF9-expressing plasmid, 200 μl of opti-MEM, and 2 μl of Lipofectamine 2000

reagent (Thermo Fisher Scientific) per 1 ml of culture medium, and cultured for 48 h. For nuclear RNA knockdown, a modified antisense or control oligonucleotide (1 μM) was transfected into 3×10^6 cells using Nucleofector technology (Lonza) 16–18 h before the assay. ASOs and siRNAs are listed in Appendix Table S1.

Western blotting

Cell lysate in 1× SDS sample buffer was boiled for 5 min, separated by SDS-PAGE, and transferred to a PVDF membrane (Millipore) by electroblotting. After incubation with primary and HRP-conjugated secondary antibodies, the signals on the membranes were developed by a chemiluminescence reaction using the ImmunoStar Kit (Wako Chemicals), detected with a ChemiDoc imaging system (BioRad), and analyzed using ImageJ software (NIH). For analysis of the phosphorylation statuses of SR proteins, the samples were separated in a SDS-PAGE gel containing Phos-tag acrylamide (Fuji Film) and then transferred to a membrane according to the manufacturer's manual. For Lambda protein phosphatase treatment, the cell lysate in 1× SDS sample buffer was precipitated by TCA, dissolved in NEBuffer for PMP (NEB) containing 1 mM $MnCl_2$ and incubated with Lambda protein phosphatase (NEB) at 30°C. Antibodies are listed in Appendix Table S1.

Quantitative and semi-quantitative RT-PCR

Total RNAs were prepared from cultured cells, subcellular fractions, or ChIRP samples using TRI Reagent or TRI Reagent LS (Molecular Research Center, Inc.), according to the manufacturer's manual. The RNAs were treated with RQ1 RNase-free DNase (Promega) according to the manufacturer's manual. First-strand cDNA was synthesized using High-Capacity cDNA Reverse Transcription Kits (Thermo Fisher Scientific). For quantitative reverse-transcription PCR (qRT-PCR), the sample and reference cDNAs were amplified using LightCycler 480 SYBR Green I Master Mix (Roche) and monitored using the LightCycler 480 System (Roche). For semi-quantitative RT-PCR**,** cDNAs were amplified by PCR to unsaturated levels, separated by electrophoresis, and stained with ethidium bromide. Images were obtained with a ChemiDoc system (BioRad) and analyzed with ImageJ software (NIH). Primers for PCR are listed in Appendix Table S2.

Nascent RNA purification

Labeling and capturing of newly synthesized RNAs was performed using the Click-iT Nascent RNA Capture Kit (Thermo Fisher Scientific), according to the

manufacturer’s protocol. Labeling was performed in the presence of 0.4 mM 5-Ethynyl Uridine (EU) for the indicated period. The purified RNAs were reverse-transcribed and analyzed by quantitative or semi-quantitative PCR as described above.

FISH and immunofluorescence

HSATIII RNA in situ hybridization and immunofluorescence were carried out as described by Aly et al (2019). Cells cultured on cover glasses were washed with ice-cold PBS and fixed in 4% PFA/PBS for 10 min at room temperature. Subsequently, the cover glasses were washed twice with ice-cold PBS and permeabilized in cold 70% ethanol for at least 1 h at 4°C. Next, the cover glasses were washed with 10% formamide/2× SSC, hybridized with a Dig-labeled HSATIII antisense oligonucleotide in hybridization buffer (10% formamide, 2× SSC, and 10% dextran) for 16 h at 37°C, incubated in 10% formamide/2× SSC for 30 min at 37°C, and then washed in 2× SSC for 5 min. After blocking in 3% BSA/TBST for 30 min, the cover glasses were incubated in 3% BSA/TBST containing an anti-dig antibody and an antibody against the protein of interest. After washing in TBST, the cover glasses were incubated in 3% BSA/TBST with Alexa 488- or Alexa 568-conjugated secondary antibodies. For NEAT1 FISH, Quasar 570-conjugated ASOs for NEAT1 were hybridized as described above. For

immunostaining, the fixed cells were permeabilized in cold PBS containing 0.1% Triton X100 for 15 min, followed by the antibody reaction as described above. Images were obtained using a confocal laser scanning microscope, FLUOVIEW FV1000 (Olympus). Probes and antibodies are listed in Appendix Table S1.

Bioinformatics analyses of RNA-seq data

Total RNAs of HeLa nuclear fractions were prepared as described above. Poly (A)+ RNA purification and library construction were performed using 200 ng of nuclear total RNAs and the Illumina TruSeq Stranded mRNA HT Sample Prep Kit. Subsequently, RNA-seq was performed using the Illumina Hiseq3000 system with the 36 bp single end method. Raw RNA-seq reads containing low quality and ambiguous bases were filtered out using cutadapt (version 1.9.1) (Martin, 2011) with the following parameters: -q 30 --max-n 0 -m 30. After this filtering, the remaining reads were mapped to the hg38 human reference genome using STAR aligner (version 2.5.3a) (Dobin, Davis et al., 2013) with the parameters --runThreadN 10 --outSAMtype BAM SortedByCoordinate --twopassMode Basic, and Gencode release27 annotation (Frankish, Diekhans et al., 2019).

For unambiguous counting of mapped reads with exon/intron resolution rather

than transcript/gene levels, a single transcript was selected per gene using CGAT scripts (version 0.3.2) (Sims, Ilott et al., 2014) with the following parameters: gtf2gtf --method=filter --filter-method=representative-transcript. In these parameters, the “representative transcript” that shared the most exons with the other transcripts in the same gene was used. In the representative transcripts, the genomic coordinates of introns were calculated from the coordinates of exons using CGAT script with the parameters gtf2gtf --method=exons2introns, and these coordinates were merged into a single GTF file for the read counting process. For each intron annotation in the GTF file, a unique ID (ENSIxxxx; this ID is named after the upstream exon ID defined as ENSExxxx in the Gencode annotation) was added; “exon” was set into the feature field (third field in GTF format) for the counting process. The mapped reads were counted using the featureCounts algorithm (subread-1.4.6) (Liao, Smyth et al., 2014) with the following parameters: -s 2 -T 10 -t exon -g exon_id. Using these count data, differential expression analysis with exon/intron resolution was conducted using DESeq2 (version 1.10.1) (Love, Huber et al., 2014) with default parameters. Using the DESeq2 results, HSATIII target introns were selected according to the following criteria: fold-change (HSATIII-KD / control) <0.5 and adjusted *p*-value <0.01.

Data analyses of RNA-seq and eCLIP

eCLIP peak data of SRSFs were obtained from the ENCODE website (ID: ENCFF214HOA, ENCFF508DKJ, ENCFF593CEQ, ENCFF944XFZ, ENCFF432ASF, ENCFF327JJE) (Van Nostrand, Pratt et al., 2016). Regions that overlapped between the SRSF9 eCLIP peaks and the HSATIII target introns/adjacent exons were counted using bedtools (v2.28.0) (Quinlan & Hall, 2010) with the following parameters: intersect -s -c –F 0.5. As the control introns for the HSATIII target introns, overlaps between the SRSF9 peaks and all introns in the representative transcripts annotated in Gencode release 27 (for details, see above section “Bioinformatics analyses of RNA-seq data”) were also investigated.

Previously reported human (U-87 MG) or mouse (mESC) detained introns were obtained from the Supplemental Data of previous studies (Boutz et al., 2015; Braun et al., 2017). The genomic coordinates (based on hg19 or mm9) of these introns were converted to hg38 coordinates using the UCSC liftOver tool (Hinrichs, Karolchik et al., 2006) with default settings. The regions that overlapped between these introns and the HSATIII target introns were counted using bedtools with the following parameter: intersect –s.

Gene ontology analysis

The gene ontology (GO) functional enrichment analyses were performed using DAVID Bioinformatics Resources 6.8 (LHRI).

Quantification and Statistical analysis

RT-PCR results were quantified using Lightcycler 480 software, version 1.5 (Roche). Semi-quantitative RT-PCR and western blot results were quantified using ImageJ software (NIH). These assays were performed on biological triplicates. FISH and IF data were quantified using ImageJ (FIJI) software. Pearson correlation colocalization analysis was performed using the Coloc 2 tool in ImageJ (FIJI) software. The statistical significance of two-group and multiple comparisons was tested using GraphPad Prism7 software (GraphPad Software), as indicated in each figure legend. Non-adjusted (two-group comparison) and adjusted (multiple comparison) P-values are indicated in each figure.

Data Availability

The RNA-seq data have been deposited in the DNA Data Bank of Japan (DDBJ) database (https://www.ddbj.nig.ac.jp/index-e.html) and assigned the identifier (DRA007304).

Acknowledgments

The authors thank Prof. Y. Suzuki (University of Tokyo) for conducting the RNA-seq analysis, Dr. N. Kataoka (University of Tokyo) for providing the SRSF9 expression plasmid, Dr. H. Maita (Hokkaido University) for providing the CHO cell line, and the members of the Hirose laboratory for valuable discussions. The computational analysis was partially performed on the NIG supercomputer at the ROIS National Institute of Genetics. This research was supported by MEXT KAKENHI grants to TH (JP26113002, JP16H06279, JP17H03630, and JP17K19335) and to NK (JP19K06478)] and by the Tokyo Biochemical Research Foundation (to T.H.).

Author contributions

KN and TH conceived and designed the study. KN conducted most of the experiments. SA and TN performed the mass spectrometry analyses. JI, GT, and KA analyzed the bioinformatics data from the RNA-seq and eCLIP experiments. KN and TH wrote the manuscript.

Conflict of interests

The authors declare no competing interests.

References

Aly MK, Ninomiya K, Adachi S, Natsume T, Hirose T (2019) Two distinct nuclear stress bodies containing different sets of RNA-binding proteins are formed with HSATIII architectural noncoding RNAs upon thermal stress exposure. Biochem Biophys Res

Commun 516: 419-423

Aubol BE, Plocinik RM, Hagopian JC, Ma CT, McGlone ML, Bandyopadhyay R, Fu XD, Adams JA (2013) Partitioning RS domain phosphorylation in an SR protein through the CLK and SRPK protein kinases. J Mol Biol 425: 2894-909

Aubol BE, Plocinik RM, Keshwani MM, McGlone ML, Hagopian JC, Ghosh G, Fu XD, Adams JA (2014) N-terminus of the protein kinase CLK1 induces SR protein hyperphosphorylation. Biochem J 462: 143-52

Banani SF, Lee HO, Hyman AA, Rosen MK (2017) Biomolecular condensates: organizers of cellular biochemistry. Nat Rev Mol Cell Biol 18: 285-298

Biamonti G, Vourc'h C (2010) Nuclear stress bodies. Cold Spring Harb Perspect Biol 2: a000695

Bonnet A, Grosso AR, Elkaoutari A, Coleno E, Presle A, Sridhara SC, Janbon G, Geli V, de Almeida SF, Palancade B (2017) Introns Protect Eukaryotic Genomes from Transcription-Associated Genetic Instability. Mol Cell 67: 608-621 e6

Boutz PL, Bhutkar A, Sharp PA (2015) Detained introns are a novel, widespread class of post-transcriptionally spliced introns. Genes Dev 29: 63-80

Braun CJ, Stanciu M, Boutz PL, Patterson JC, Calligaris D, Higuchi F, Neupane R, Fenoglio S, Cahill DP, Wakimoto H, Agar NYR, Yaffe MB, Sharp PA, Hemann MT, Lees JA (2017) Coordinated Splicing of Regulatory Detained Introns within Oncogenic Transcripts Creates an Exploitable Vulnerability in Malignant Glioma. Cancer Cell 32: 411-426 e11

Bullock AN, Das S, Debreczeni JE, Rellos P, Fedorov O, Niesen FH, Guo K, Papagrigoriou E, Amos AL, Cho S, Turk BE, Ghosh G, Knapp S (2009) Kinase domain insertions define distinct roles of CLK kinases in SR protein phosphorylation. Structure 17: 352-62

Cao W, Jamison SF, Garcia-Blanco MA (1997) Both phosphorylation and dephosphorylation of ASF/SF2 are required for pre-mRNA splicing in vitro. RNA 3:

1456-67

Castello A, Fischer B, Eichelbaum K, Horos R, Beckmann BM, Strein C, Davey NE, Humphreys DT, Preiss T, Steinmetz LM, Krijgsveld J, Hentze MW (2012) Insights into RNA biology from an atlas of mammalian mRNA-binding proteins. Cell 149: 1393-406

Chu C, Quinn J, Chang HY (2012) Chromatin isolation by RNA purification (ChIRP). J Vis Exp

Chujo T, Yamazaki T, Hirose T (2016) Architectural RNAs (arcRNAs): A class of long noncoding RNAs that function as the scaffold of nuclear bodies. Biochim Biophys Acta 1859: 139-46

Clemson CM, Hutchinson JN, Sara SA, Ensminger AW, Fox AH, Chess A, Lawrence JB (2009) An architectural role for a nuclear noncoding RNA: NEAT1 RNA is essential for the structure of paraspeckles. Mol Cell 33: 717-26

Colwill K, Pawson T, Andrews B, Prasad J, Manley JL, Bell JC, Duncan PI (1996) The Clk/Sty protein kinase phosphorylates SR splicing factors and regulates their intranuclear distribution. EMBO J 15: 265-75

Denegri M, Chiodi I, Corioni M, Cobianchi F, Riva S, Biamonti G (2001) Stress-induced nuclear bodies are sites of accumulation of pre-mRNA processing factors. Mol Biol Cell 12: 3502-14

Denegri M, Moralli D, Rocchi M, Biggiogera M, Raimondi E, Cobianchi F, De Carli L, Riva S, Biamonti G (2002) Human chromosomes 9, 12, and 15 contain the nucleation sites of stress-induced nuclear bodies. Mol Biol Cell 13: 2069-79

Dobin A, Davis CA, Schlesinger F, Drenkow J, Zaleski C, Jha S, Batut P, Chaisson M, Gingeras TR (2013) STAR: ultrafast universal RNA-seq aligner. Bioinformatics 29: 15-21

Dominguez D, Tsai YH, Weatheritt R, Wang Y, Blencowe BJ, Wang Z (2016) An extensive program of periodic alternative splicing linked to cell cycle progression. Elife 5

Duncan PI, Howell BW, Marius RM, Drmanic S, Douville EM, Bell JC (1995) Alternative splicing of STY, a nuclear dual specificity kinase. J Biol Chem 270: 21524-31

Duncan PI, Stojdl DF, Marius RM, Bell JC (1997) In vivo regulation of alternative pre-mRNA splicing by the Clk1 protein kinase. Mol Cell Biol 17: 5996-6001

Fedorov O, Huber K, Eisenreich A, Filippakopoulos P, King O, Bullock AN, Szklarczyk D, Jensen LJ, Fabbro D, Trappe J, Rauch U, Bracher F, Knapp S (2011) Specific CLK inhibitors from a novel chemotype for regulation of alternative splicing. Chem Biol 18: 67-76

Frankish A, Diekhans M, Ferreira AM, Johnson R, Jungreis I, Loveland J, Mudge JM, Sisu C, Wright J, Armstrong J, Barnes I, Berry A, Bignell A, Carbonell Sala S, Chrast J, Cunningham F, Di Domenico T, Donaldson S, Fiddes IT, Garcia Giron C et al. (2019) GENCODE reference annotation for the human and mouse genomes. Nucleic Acids Res 47: D766-D773

Gill J, Park Y, McGinnis JP, Perez-Sanchez C, Blanchette M, Si K (2017) Regulated Intron Removal Integrates Motivational State and Experience. Cell 169: 836-848 e15

Graveley BR (2000) Sorting out the complexity of SR protein functions. RNA 6: 1197-211

Gui JF, Lane WS, Fu XD (1994) A serine kinase regulates intracellular localization of splicing factors in the cell cycle. Nature 369: 678-82

Guil S, Caceres JF (2007) Stressful splicing. Mol Cell 28: 180-1

Hinrichs AS, Karolchik D, Baertsch R, Barber GP, Bejerano G, Clawson H, Diekhans M, Furey TS, Harte RA, Hsu F, Hillman-Jackson J, Kuhn RM, Pedersen JS, Pohl A, Raney BJ, Rosenbloom KR, Siepel A, Smith KE, Sugnet CW, Sultan-Qurraie A et al. (2006) The UCSC Genome Browser Database: update 2006. Nucleic Acids Res 34: D590-8

Huang Y, Yario TA, Steitz JA (2004) A molecular link between SR protein dephosphorylation and mRNA export. Proc Natl Acad Sci U S A 101: 9666-70

Hussong M, Kaehler C, Kerick M, Grimm C, Franz A, Timmermann B, Welzel F, Isensee J, Hucho T, Krobitsch S, Schweiger MR (2017) The bromodomain protein BRD4 regulates splicing during heat shock. Nucleic Acids Res 45: 382-394

Jarmuz M, Glotzbach CD, Bailey KA, Bandyopadhyay R, Shaffer LG (2007) The Evolution of satellite III DNA subfamilies among primates. Am J Hum Genet 80: 495-501

Jolly C, Konecny L, Grady DL, Kutskova YA, Cotto JJ, Morimoto RI, Vourc'h C (2002) In vivo binding of active heat shock transcription factor 1 to human chromosome 9 heterochromatin during stress. J Cell Biol 156: 775-81

Jolly C, Metz A, Govin J, Vigneron M, Turner BM, Khochbin S, Vourc'h C (2004) Stress-induced transcription of satellite III repeats. J Cell Biol 164: 25-33

Jolly C, Morimoto R, Robert-Nicoud M, Vourc'h C (1997) HSF1 transcription factor concentrates in nuclear foci during heat shock: relationship with transcription sites. J Cell Sci 110 (Pt 23): 2935-41

Jolly C, Usson Y, Morimoto RI (1999) Rapid and reversible relocalization of heat shock factor 1 within seconds to nuclear stress granules. Proc Natl Acad Sci U S A 96: 6769-74

Kawaguchi T, Tanigawa A, Naganuma T, Ohkawa Y, Souquere S, Pierron G, Hirose T (2015) SWI/SNF chromatin-remodeling complexes function in noncoding RNA-dependent assembly of nuclear bodies. Proc Natl Acad Sci U S A 112: 4304-9

Keshwani MM, Hailey KL, Aubol BE, Fattet L, McGlone ML, Jennings PA, Adams JA (2015) Nuclear protein kinase CLK1 uses a non-traditional docking mechanism to select physiological substrates. Biochem J 472: 329-38

Kinoshita E, Kinoshita-Kikuta E, Matsubara M, Yamada S, Nakamura H, Shiro Y, Aoki Y, Okita K, Koike T (2008) Separation of phosphoprotein isotypes having the same number of phosphate groups using phosphate-affinity SDS-PAGE. Proteomics 8: 2994-3003

Liao Y, Smyth GK, Shi W (2014) featureCounts: an efficient general purpose program

for assigning sequence reads to genomic features. Bioinformatics 30: 923-30

Long JC, Caceres JF (2009) The SR protein family of splicing factors: master regulators of gene expression. Biochem J 417: 15-27

Love MI, Huber W, Anders S (2014) Moderated estimation of fold change and dispersion for RNA-seq data with DESeq2. Genome Biol 15: 550

Mahl P, Lutz Y, Puvion E, Fuchs JP (1989) Rapid effect of heat shock on two heterogeneous nuclear ribonucleoprotein-associated antigens in HeLa cells. J Cell Biol 109: 1921-35

Martin M (2011) Cutadapt removes adapter sequences from high-throughput sequencing reads. In EMBnet journal, pp 10-12.

Mauger O, Lemoine F, Scheiffele P (2016) Targeted Intron Retention and Excision for Rapid Gene Regulation in Response to Neuronal Activity. Neuron 92: 1266-1278

Metz A, Soret J, Vourc'h C, Tazi J, Jolly C (2004) A key role for stress-induced satellite III transcripts in the relocalization of splicing factors into nuclear stress granules. J Cell Sci 117: 4551-8

Mili S, Shu HJ, Zhao Y, Pinol-Roma S (2001) Distinct RNP complexes of shuttling hnRNP proteins with pre-mRNA and mRNA: candidate intermediates in formation and export of mRNA. Molecular and cellular biology 21: 7307-19

Morgan JT, Fink GR, Bartel DP (2019) Excised linear introns regulate growth in yeast. Nature 565: 606-611

Naganuma T, Nakagawa S, Tanigawa A, Sasaki YF, Goshima N, Hirose T (2012) Alternative 3'-end processing of long noncoding RNA initiates construction of nuclear paraspeckles. EMBO J 31: 4020-34

Naro C, Jolly A, Di Persio S, Bielli P, Setterblad N, Alberdi AJ, Vicini E, Geremia R, De la Grange P, Sette C (2017) An Orchestrated Intron Retention Program in Meiosis Controls Timely Usage of Transcripts during Germ Cell Differentiation. Dev Cell 41: 82-93 e4

Nayler O, Stratling W, Bourquin JP, Stagljar I, Lindemann L, Jasper H, Hartmann AM, Fackelmayer FO, Ullrich A, Stamm S (1998) SAF-B protein couples transcription and pre-mRNA splicing to SAR/MAR elements. Nucleic Acids Res 26: 3542-9

Ninomiya K, Kataoka N, Hagiwara M (2011) Stress-responsive maturation of Clk1/4 pre-mRNAs promotes phosphorylation of SR splicing factor. J Cell Biol 195: 27-40

Parenteau J, Maignon L, Berthoumieux M, Catala M, Gagnon V, Abou Elela S (2019) Introns are mediators of cell response to starvation. Nature 565: 612-617

Preussner M, Goldammer G, Neumann A, Haltenhof T, Rautenstrauch P, Muller-McNicoll M, Heyd F (2017) Body Temperature Cycles Control Rhythmic Alternative Splicing in Mammals. Mol Cell 67: 433-446 e4

Quinlan AR, Hall IM (2010) BEDTools: a flexible suite of utilities for comparing genomic features. Bioinformatics 26: 841-2

Shepard PJ, Hertel KJ (2009) The SR protein family. Genome Biol 10: 242

Shi Y, Manley JL (2007) A complex signaling pathway regulates SRp38 phosphorylation and pre-mRNA splicing in response to heat shock. Molecular cell 28: 79-90

Shin C, Feng Y, Manley JL (2004) Dephosphorylated SRp38 acts as a splicing repressor in response to heat shock. Nature 427: 553-8

Simard MJ, Chabot B (2002) SRp30c is a repressor of 3' splice site utilization. Mol Cell Biol 22: 4001-10

Sims D, Ilott NE, Sansom SN, Sudbery IM, Johnson JS, Fawcett KA, Berlanga-Taylor AJ, Luna-Valero S, Ponting CP, Heger A (2014) CGAT: computational genomics analysis toolkit. Bioinformatics 30: 1290-1

Tai HH, Geisterfer M, Bell JC, Moniwa M, Davie JR, Boucher L, McBurney MW (2003) CHD1 associates with NCoR and histone deacetylase as well as with RNA splicing proteins. Biochem Biophys Res Commun 308: 170-6

Tanabe H, Nakagawa Y, Minegishi D, Hashimoto K, Tanaka N, Oshimura M, Sofuni T, Mizusawa H (2000) Human monochromosome hybrid cell panel characterized by FISH in the JCRB/HSRRB. Chromosome Res 8: 319-34

Valgardsdottir R, Chiodi I, Giordano M, Cobianchi F, Riva S, Biamonti G (2005) Structural and functional characterization of noncoding repetitive RNAs transcribed in stressed human cells. Mol Biol Cell 16: 2597-604

Van Nostrand EL, Pratt GA, Shishkin AA, Gelboin-Burkhart C, Fang MY, Sundararaman B, Blue SM, Nguyen TB, Surka C, Elkins K, Stanton R, Rigo F, Guttman M, Yeo GW (2016) Robust transcriptome-wide discovery of RNA-binding protein binding sites with enhanced CLIP (eCLIP). Nat Methods 13: 508-14

Weighardt F, Cobianchi F, Cartegni L, Chiodi I, Villa A, Riva S, Biamonti G (1999) A novel hnRNP protein (HAP/SAF-B) enters a subset of hnRNP complexes and relocates in nuclear granules in response to heat shock. J Cell Sci 112 (Pt 10): 1465-76

Xiao SH, Manley JL (1997) Phosphorylation of the ASF/SF2 RS domain affects both protein-protein and protein-RNA interactions and is necessary for splicing. Genes Dev 11: 334-44

Yamamoto K, Furukawa MT, Fukumura K, Kawamura A, Yamada T, Suzuki H, Hirose T, Sakamoto H, Inoue K (2016) Control of the heat stress-induced alternative splicing of a subset of genes by hnRNP K. Genes Cells 21: 1006-14

Yasuda K, Nakai A, Hatayama T, Nagata K (1995) Cloning and expression of murine high molecular mass heat shock proteins, HSP105. J Biol Chem 270: 29718-23

Figure legends

Figure 1. HSATIII lncRNAs control intron retention of a specific set of genes

A Outline of the screening for HSATIII-regulated genes during thermal stress recovery. HeLa cells were transfected with a HSATIII ASO (HSATIII KD) or HSATIII sense oligonucleotide (control), exposed to thermal stress. Nuclear polyA(+) RNAs were analyzed by next-generation sequencing (NGS). NGS data have been deposited in the DDBJ Sequence Read Archive (DRA) (accession number: DRA007304).

B HSATIII ASO-mediated depletion of nSBs. Thermal stress-exposed HeLa cells (42°C for 2 h and recovery for 1 h at 37°C) were visualized by HSATIII-FISH and immunofluorescence using an anti-SAFB antibody or anti-HNRNPM antibody. The nuclei were stained with DAPI. Scale bar: 10 μm.

C qRT-PCR-validation of HSATIII knockdown. The graph shows the qRT-PCR level of HSATIII RNAs in control and HSATIII knockdown cells under three conditions: 37°C, 42°C for 2 h, and thermal stress followed by recovery at 37°C for 1 h (Recovery). Expression levels were calculated as ratios to *GAPDH* mRNA and were normalized to the levels in control cells under thermal stress conditions (42°C for 2 h). Data are shown as the mean±SD (n=3). HSATIII RNAs ratios (%) are indicated.

D MA-plot (log2 fold-change over the average expression level) of all detected introns

in HSATIII KD and control cells (n=3). The introns with significant changes in their expression levels (adjusted p-value < 0.01) are shown as green dots. Among these introns, up-regulated (log2 fold-change > 1) and down-regulated (log2 fold-change < -1) introns are shown with magenta and light blue dots, respectively. Genes and introns that were experimentally validated in subsequent experiments are indicated as gene symbol-i (intron) #. Total numbers of introns and genes utilized were 144769 and 32623, respectively.

E The numbers of introns and exons that were affected by HSATIII knockdown (fold change>2).

F, G Examples of RNA-seq read maps of HSATIII target RNAs. Affected introns and exons are indicated by blue (down-regulated upon HSATIII knockdown) and magenta (up-regulated) boxes.

H Cumulative frequency curves of the lengths of adjacent exons of 399 HSATIII-up-regulated internal introns. The lengths of whole annotated internal introns are shown as a reference.

Figure 2. HSATIII lncRNAs control intron retention by regulating splicing.

A Validation of HSATIII target introns by qRT-PCR. The graphs show the relative

amounts of the intron-retaining (IR) (upper) and spliced (lower) forms in control and HSATIII knockdown cells under three conditions: 37°C (normal), 42°C for 2 h (thermal stress), and thermal stress followed by recovery at 37°C for 1 h. Expression levels were calculated as the ratio of each RNA to *GAPDH* mRNA and were normalized to the levels in control cells under normal conditions (37°C). Data are shown as the mean±SD (n=3); *p<0.05 (Sidak's multiple comparison test).

B Nuclear localization of the intron-retaining RNAs. The relative amounts of intron-retaining RNAs in the nuclear and cytoplasmic fractions were quantified by qRT-PCR and are represented as the ratio (% of the total). *GAPDH* mRNA and U1 snRNA were used as cytoplasmic and nuclear controls, respectively. Data are shown as the mean±SD (n=3).

C Overview of the qRT-PCR analysis of newly synthesized RNA within 1 h after thermal stress removal. CHX, Cycloheximide; EU, 5-Ethynyl uridine

D, E The levels of HSATIII target introns in newly synthesized RNAs within 1 h after thermal stress removal, as determined by qRT-PCR. The graphs show the changes in the expression levels of the intron-retaining (IR) (D) and spliced (E) forms. Expression levels were calculated as the ratio of each RNA to *GAPDH* mRNA and were normalized to the level in the control cells. Data are shown as the mean±SD (n=3); *p<0.05

(multiple t-test modified by Holm-Sidak's method).

Figure 3. The HSATIII lncRNA is necessary and sufficient to promote nuclear intron retention

A Splicing isoforms of the *CLK1* pre-mRNA. The retained introns are indicated by red lines. An asterisk indicates the position of the premature termination codon in the nonsense-mediated mRNA decay-targeted isoform.

B Time course analysis of the splicing pattern of *CLK1* pre-mRNAs in control and HSATIII knockdown (HSATIII KD) cells by semi-quantitative RT-PCR. Arrows indicate the positions of PCR primers. The *GAPDH* mRNA was used as an internal control.

C Quantification of the data shown in (B). Data are shown as the mean±SD (n=3); *p<0.05 (Sidak's multiple comparison test).

D Thermal stress-induced expression of HSATIII in CHO (His9) cells. The cells were visualized by HSATIII-FISH (green), and the nuclei were stained with DAPI (blue). Scale bar: 10 μm.

E Ectopic HSATIII-induced nSB assembly in CHO (His9) cells. The nSBs (yellow arrowheads) were visualized by HSATIII-FISH and immunofluorescence using an anti-SRSF1 antibody. The nuclei were stained with DAPI. Scale bar: 10 μm.

F Time course analysis of the splicing pattern of Chinese hamster *Clk1* pre-mRNAs in control (CHO) and CHO (His9) cells by semi-quantitative RT-PCR. Arrows indicate the positions of PCR primers. The *GAPDH* mRNA was used as an internal control.

G Quantification of the data shown in (F). Data are shown as the mean±SD (n=3); **p*<0.05 (Sidak's multiple comparison test).

H The effect of HSATIII knockdown on pooling of intron-retaining RNAs in control (CHO) and CHO (His9) cells (42°C for 2 h and recovery for 2 h at 37°C). Arrows indicate the positions of PCR primers.

Figure 4. Identification of HSATIII-interacting proteins by ChIRP.

A Overview of the ChIRP procedure used to identify HSATIII-interacting proteins in thermal stress-exposed cells. HSATIII-interacting proteins were crosslinked and captured with a biotinylated HSATIII ASO. As a negative control, the same procedure was performed using control (37°C) cells and/or a control probe.

B RT-PCR validation of the specific precipitation of HSATIII by ChIRP. The NEAT1 ncRNA and *GAPDH* mRNA were used as negative controls. Input: 100%.

C Silver staining of the coprecipitated proteins. The predicted mobilities of five known nSB proteins are indicated. Input: 0.1%.

D Western blot analyses of proteins identified by the HSATIII-ChIRP experiment.

Known nSB proteins (SAFB, SRSF1, SRSF7, SRSF9, and HNRNPM) were used as positive controls, and ELAVL1, PSPC1 and α-tubulin were used as negative controls. SRSF3, SRSF5, TRA2B and THRAP3 are newly identified nSB components.

E–G Colocalization of novel nSB proteins with HSATIII. Endogenous TRA2B (E), THRAP3 (F), and FLAG-tagged PPHLN1 (G) were stained with anti-TRA2B, anti-THRAP3, and anti-FLAG antibodies, respectively. HSATIII was visualized by RNA-FISH using a dig-labeled HSATIII ASO, and the nuclei were stained with DAPI. Scale bar: 10 μm.

Figure 5. CLK1 is recruited to nSBs during thermal stress recovery

A Specific interaction of CLK1 with HSATIII during thermal stress recovery. HSATIII-ChIRP at various time points during and after thermal stress exposure. Endogenous CLK1, SRSF7, and SRSF9 were detected using anti-CLK1, anti-SRSF7, and anti-SRSF9 antibodies, respectively. HSATIII was detected by ChIRP-RNA purification, followed by RT-PCR. Input: 0.1% for CLK1, 1% for SRSF7 and SRSF9, and 100% for HSATIII.

B The domain structures of wild-type (WT) CLK1, the catalytically inactive mutant (CLK1 KR), and the N- and C-terminal partial fragments (CLK1ΔC and CLK1ΔN).

C Specific interaction of HSATIII with CLK1 proteins during stress recovery. HSATIII-ChIRP/western blotting was performed using HeLa cells expressing FLAG-CLK1 WT or the KR mutant. FLAG-tagged CLK1 and SRSF9 were detected by western blotting using an anti-FLAG and an anti-SRSF9 antibody, respectively. HSATIII was detected by ChIRP followed by RT-PCR. Input: 1% for western blotting, 100% for RT-PCR.

D Re-translocation of FLAG-CLK1 to nSBs after thermal stress removal. HeLa cells were transfected with a FLAG-CLK1 expression vector, cultured for 16 h, and then exposed to thermal stress (42°C for 2 h) with or without recovery (37°C for 1 h). FLAG-CLK1 was visualized with an anti-FLAG antibody. Nuclear stress bodies and nuclei were visualized by HSATIII-FISH and DAPI staining, respectively. Scale bar: 10 μm.

E Box plot of colocalization correlation coefficients between HSATIII and FLAG-CLK1 WT. The first and third quartiles are the ends of the box, the median is indicated by the vertical line in the box, and the minimum and maximum are the ends of the whiskers.

(n=20 nuclei for each condition). *p<0.05 (Mann–Whitney U-test).

F Recovery phase-specific interaction of HSATIII with the CLK1 N-terminal region. HSATIII-ChIRP/western blotting was performed on HeLa cells expressing

FLAG-CLK1ΔC or FLAG-CLK1ΔN using the same procedure as in (C). Asterisk: an unidentified partial fragment of FLAG-CLK1ΔN.

G, H Dependency of SRSF9 on the interaction of CLK1 (G) and CLK1ΔC (H) with HSATIII. HSATIII-ChIRP was performed using control and SRSF9-depleted cells expressing FLAG-CLK1 proteins (42°C for 2 h and recovery for 1 h at 37°C). Input: 1%. Graphs represent coprecipitation ratios of FLAG-CLK1 proteins to HSATIII in the control and SRSF9-depleted cells. Data are shown as the mean±SD (n=3); *p<0.05 (Welch's t-test).

Figure 6. The HSATIII lncRNA accelerates CLK1-dependent re-phosphorylation of SRSF9

A Localization of SRSF9 with HSATIII during thermal stress and recovery. Scale bar: 10 μm.

B Recovery phase-specific colocalization of CLK1 and SRSF9. HeLa cells were transfected with a FLAG-CLK1 expression vector, cultured for 16 h, and exposed to thermal stress (42°C for 2 h) followed by recovery (37°C for 1 h). FLAG-CLK1 and SRSF9 were co-stained using anti-FLAG and anti-SRSF9 antibodies, respectively, and the nuclei were stained with DAPI. Scale bar: 10 μm.

C Box plot of colocalization correlation coefficients between SRSF9 and FLAG-CLK1 WT. The first and third quartiles are the ends of the box, the median is indicated with a vertical line in the box, and the minimum and maximum are the ends of the whiskers. (n=20 nuclei for each condition). *p<0.05 (Mann–Whitney U-test).

D Scheme of sampling references for analysis of the phosphorylation states of SRSF9 in (F). The CLK1 inhibitor KH-CB19 (10 μM) or DMSO as a control was administrated during the recovery period. The numbers correspond to the lane numbers in (F).

E Conditions tested in the time course analysis of the phosphorylation states of SR proteins. HeLa cells were transfected with a HSATIII ASO or control SO, cultured for 16 h, exposed to thermal stress (42°C for 2 h), and cultured at 37°C for the indicated period.

F The effect of HSATIII knockdown on time course-dependent changes in SRSF9 phosphorylation. The phosphorylation states were estimated by Phos-tag SDS-PAGE, followed by western blotting using an anti-SRSF9 antibody. SRSF9 detected by western blotting of a normal SDS-PAGE gel is shown in the bottom panel. The arrows and arrowheads indicate the normal phosphorylated forms and thermal stress-induced hypo- and de-phosphorylated forms, respectively.

G Quantification of the data shown in (F). Graphs show the time-course changes in four representative SRSF9 phosphorylated forms in (F). Relative levels of band intensity

were calculated as the ratio of each band to α-tubulin and were normalized to those of control at 37°C (bands (a) and (b)) and 42°C (bands (c) and (d)). Since band (d) partially overlapped with the other band (asterisk in (F)) at 37°C and recovery 4h, band (d) at those time points was not measured. Data are shown as the mean±SD (n=3); *p<0.05 (Sidak's multiple comparison test).

H The re-phosphorylation status of SRSF9 within nSBs. Also, see Figure EV4G. Phosphorylated (arrows) and hypo- and de-phosphorylated (arrowheads) SRSF9 in the nSB fractions (lanes 4, 6, and 8) were analyzed by western blotting on Phos-tag gels. KH-CB19 (10 μM) or DMSO as a control was administrated during the recovery period. The lower panel shows a shorter exposure image of the phosphorylated forms. The asterisks indicate bands different from band (a) or (d). Input: 5%.

I Quantification of the data shown in (H). Relative band intensities were calculated as the ratios of each band to total SRSF9 detected by western blotting of a standard SDS-PAGE, and were normalized to those at 42°C. Data are shown as the mean±SD (n=4) (Dunnett's multiple comparison test) .

Figure 7. The role of SRSF9 re-phosphorylation in controlling HSATIII-dependent intron retention

A, B　Validation of the effect of SRSF9 on retention/splicing of HSATIII target introns by qRT-PCR. The relative expression levels of intron-retaining (IR) forms (A) and spliced forms (B) of newly transcribed RNAs during the recovery period are shown. See also the scheme in Figure 2C. Expression levels were calculated as the ratio of each RNA to *GAPDH* mRNA and were normalized to the control. Data are shown as the mean±SD (n=3); *p<0.05 (multiple t-test modified by Holm-Sidak's method).

C, D　Time course analysis of the splicing patterns of *CLK1* and *TAF1D* intron-retaining RNAs in control and HSATIII knockdown cells by semi-quantitative RT-PCR. Arrows indicate the positions of primers for RT-PCR. *GAPDH* mRNA was used as an internal control. The experiment was performed in triplicate. Quantification of the data shown in (C), Data are shown as the mean±SD (n=3); *p<0.05 (Sidak's multiple comparison test).

E　Scheme for analyzing the effect of CLK1 inhibition on intron retention by newly transcribed RNAs after stress removal. CHX, Cycloheximide; EU, 5-Ethynyl uridine.

F　Validation of the requirement of CLK1 catalytic activity for promotion of intron retention by qRT-PCR. Data are shown as the mean±SD (n=3). P values (multiple t-test modified by Holm-Sidak's method) are shown.

G　The diagrams show the domain structures of wild-type (WT) and mutant (mut) SRSF9, in which all SR/SP dipeptides were replaced by AR/AP. FLAG-SRSF9-WT and

FLAG-SRSF9-mut were extracted from transfected HeLa cells under normal (37°C) and thermal stress (42°C for 2 h) conditions, separated in a Phos-tag gel, and detected by western blot using an anti-FLAG antibody. The arrowhead indicates the thermal stress-induced de-phosphorylated form of FLAG-SRSF9-WT.

H, I The role of phosphorylation of SRSF9 on splicing of the *TAF1D* (H) *and DNAJB9* (I) reporters. Each *s*plicing reporter plasmid was transfected into HeLa cells along with a siRNA (control or SRSF9-specific) and a siRNA-resistant SRSF9-WT or SRSF9-mut expression plasmid (or pEGFP-C1 vector as the empty vehicle (-)) 48 h before the assay. Semi-quantitative RT-PCR analyses revealed the splicing patterns of the reporter RNAs purified from the thermal stress-exposed cells (42°C for 2 h and 37°C for 1 h). The positions of the PCR primers are indicated by arrows. Graphs represent the relative changes in the spliced/unspliced ratios, normalized to the control sample with control siRNA and empty plasmid (-). Data are shown as the mean±SD (n=3); *p<0.05 (Dunnett's multiple comparison test).

J A model for the function of nSBs in splicing control. Thermal stress-induced HSATIII integrates subsets of de-phosphorylated SRSFs and SR-related proteins. After stress removal, CLK1 relocates to nSBs to promote rapid re-phosphorylation of the sequestrated SRSFs, especially SRSF9. Re-phosphorylated SRSF9 suppresses

splicing of target introns to accumulate intron-retaining RNAs in the nucleus.

Expanded View Figure legends

Figure EV1 Effect of HSATIII knockdown on other nuclear bodies and gene expression

A, B Normal assembly of nuclear speckles upon HSATIII knockdown. 16 hours after HSATIII ASO transfection, HeLa cells were exposed to thermal stress (42°C for 2 hours followed by recovery for 1 hour at 37°C) and stained using anti-SRSF2 antibody with the HSATIII-FISH probe (A) or anti-SRSF3 antibody (B). Nuclei were stained with DAPI. (Scale bar: 10 μm)

C Normal assembly of nuclear speckles upon HSATIII knockdown. 16 hours after HSATIII ASO transfection, HeLa cells were exposed to thermal stress and stained using NEAT1 ASOs and anti-SFPQ antibody as paraspeckle markers. (Scale bar: 10 μm)

D, E Box plot of total area of nuclear speckles (D) and paraspeckles (E) in each nucleus. Nuclear speckles, paraspeckles, and nuclei areas are defined by binarized images of SRSF2, NEAT1, and DAPI, respectively. Mean is indicated by X (n=39 (SRSF2, control), 44 (SRSF2, HSATIII KD), 30 (NEAT1, control), 50 (NEAT1, HSATIII KD) nuclei). The first and third quartiles are the ends of the box, the median is indicated with the vertical line in the box, and the minimum and maximum are the ends of the whiskers. The outliers are indicated with open circles. p-values (Mann–Whitney U-test) are shown above the graphs.

F MA-plot (log2 fold-change over average expression level) of all detected exons (n=3). Significant change (green), significant and >2-fold increase (magenta), and decrease (light blue). Total numbers of exons and genes utilized are 162989 and 32623, respectively.

Figure EV2 Effect of HSATIII knockdown on intron retention of *TAF1D* and *DNAJB9* pre-mRNAs

A Splicing isoforms of *TAF1D and DNAJB9*. The retained introns are indicated by red lines. An asterisk indicates the position of the premature termination codon (PTC) in the NMD-targeted isoform.

B Time course analysis of splicing pattern of *TAF1D* and *DNAJB9* pre-mRNAs in control and HSATIII knockdown (HSATIII KD) cells by semi-quantitative RT-PCR. Arrows indicate the positions of PCR primers. *GAPDH* mRNA was used as internal control.

C Specificity of the HSATIII-dependent splicing control. Semi-quantitative RT-PCR validation of the splicing pattern of newly synthesized RNAs within 1 hour after thermal stress removal (see also Figure 2C). Arrows indicate the positions of PCR primers. *CLK1* and *GAPDH* pre-mRNAs were used as positive and internal controls,

respectively.

Figure EV3 Recruitment of N-terminal IDRs of CLK family proteins to nSBs and nuclear speckles.

A-H　HeLa cells were transfected with FLAG-CLK1 expression plasmid, cultured for 16 hours, and exposed to thermal stress (42°C for 2 hours) followed by recovery (37°C for 1 hour). FLAG-tagged CLK1 or its mutant (see also Figure 5B) was visualized with anti-FLAG antibody. nSBs (A, E) or nuclear speckles (B, F) and nuclei were visualized by HSATIII-FISH, IF using the anti-SRSF2 antibody, and with DAPI, respectively. (Scale bar: 10 μm). Box plots (C, D, G, H) of correlation coefficients between localization of FLAG-tagged CLK1 proteins and HSATIII (C, G) or SRSF2 (D, H). The first and third quartiles are the ends of the box, the median is indicated with the vertical line in the box, and the minimum and maximum are the ends of the whiskers. The outliers are indicated with open circles. *p<0.05 (Mann–Whitney U-test (C,G), Kruskal-Wallis test, followed by Dunn's multiple comparison test (D, H)) (n=20 nuclei (C, G, and H), n=15 (37°C), n=14 (42°C 2h), and n=16 nuclei (42°C 2 h followed by recovery for 1 hour at 37°C (D)).I Western blot of nuclear and cytoplasmic fractions of HeLa cells expressing FLAG-CLK1 truncated protein. FLAG-CLK1 proteins were detected using anti-FLAG antibody.

SRSF9 and α-tubulin were used as nuclear and cytoplasmic fraction controls, respectively. Asterisk; an unidentified partial fragment of FLAG-CLK1ΔN.

J Specific interaction of CLK family proteins with HSATIII during stress recovery. HSATIII-ChIRP was performed in thermal stress-exposed HeLa cells (42°C for 2 hours followed by recovery for 1 hour at 37°C) expressing FLAG-CLK1ΔC, CLK2ΔC and CLK4ΔC. FLAG-tagged proteins and endogenous SRSF9, used as a ChIRP control, were detected by western blotting using anti-FLAG and anti-SRSF9 antibody, respectively. Input (1%).

K Colocalization of FLAG-CLK2 ΔC and FLAG-CLK4 ΔC with HSATIII in thermal stress-exposed HeLa cells (42 °C for 2 hours followed by recovery for 1 hour at 37 °C)(Scale bar: 10 μm).

Figure EV4 HSATIII-dependent localization and phosphorylation of nSB-localizing SRSFs.

A The effect of HSATIII knockdown on SRSF9 localization. HeLa cells were transfected with HSATIII ASO (HSATIII KD) or control ASO (control), cultured for 16 hours and exposed to thermal stress (42 °C for 2 hours and 37 °C for 1 hour). The cells were stained by HSATIII-FISH, IF using SRSF9 antibody, and DAPI (Scale bar: 10 μm).

B, C The subnuclear distribution of nSBs and nuclear speckles. HeLa cells (42°C for 2 h and 37°C for 1 h) were stained with an anti-SRSF9 antibody, an anti-SRSF2 antibody, and a HSATIII-FISH probe. The nuclei were stained with DAPI. (Scale bar: 10 μm).

D Box plot of colocalization correlation coefficient among SRSF2, SRSF9 and HSATIII in HeLa nuclei (42°C for 2 h and 37°C for 1 h). The first and third quartiles are the ends of the box, the median is indicated with the vertical line in the box, and the minimum and maximum are the ends of the whiskers. The outliers are indicated with open circles. (n=20 nuclei for each). *p<0.05 (Kruskal-Wallis test followed by Dunn's multiple comparison test).

E The effect of HSATIII knockdown on time course-dependent changes in SRSF1 phosphorylation. The phosphorylation states were estimated by Phos-tag SDS-PAGE, followed by western blotting with an anti-SRSF1 antibody. SRSF1 detected by western blotting of a normal SDS-PAGE gel is shown in the bottom panel. The arrow and bracket indicate the normal phosphorylated forms and thermal stress-induced hypo- and de-phosphorylated forms, respectively.

F Phosphorylation states of SRSFs. SRSFs with longer RS domains were detected by standard SDS-PAGE western blotting with pan-phospho SR antibody (1H4) in HSATIII KD and control cells under the different temperature conditions shown above the panel.

α-tubulin is a loading control.

G Scheme of Phos-tag western blotting coupled with HSATIII-ChIRP used to validate the phosphorylation states of SRSF9 within nSBs.

H Standard SDS-PAGE of the HSATIII-ChIRP samples, followed by western blotting.

I Phos-tag SDS-PAGE of the HSATIII-ChIRP samples, followed by western blotting. SRSF1 was detected with anti-SRSF1 antibody. The bottom panel shows the emphasized images. Input (5 %). The arrow and bracket indicate the normal phosphorylated forms and thermal stress-induced hypo- and de-phosphorylated forms, respectively.

J Phos-tag western blotting of SRSF1 and SRSF9 upon phosphatase treatment. HeLa cell proteins were treated with Lambda protein phosphatase for the indicated periods. An arrow, an arrowhead, and asterisks with bracket indicate the original position, completely-dephosphorylated and transiently-increased partially-dephosphorylated bands, respectively.

Figure EV5 Intron retention controlled by SRSF9

A Western blot validation of SRSF knockdown. HeLa cells were transfected with each Stealth siRNA, cultured for 48 hours, and analyzed by western blot using anti-SRSF1,

anti-SRSF7, and anti-SRSF9 antibodies. α-tubulin was detected as a loading control.

B Normal assembly of nSBs in SRSF7 or SRSF9 knockdown cells. 48 hours after siRNA transfection, HeLa cells were exposed to thermal stress and stained by HSATIII-FISH. Nuclei were stained with DAPI (Scale bar: 10 μm).

C Quantification of (B). Box plot represents relative HSATIII intensities in nuclei. Mean is indicated by X. The first and third quartiles are the ends of the box, the median is indicated with the vertical line in the box, and the minimum and maximum are the ends of the whiskers. The outliers are indicated with open circles. (n=40 nuclei for each) *p<0.05 (Kruskal-Wallis test followed by Dunn's multiple comparison test).

D SRSFs eCLIP tag on the retaining introns and adjacent exons of *CLK1* and *TAF1D*.

E The amino acid sequence of human SRSF9. In the SRSF9 dephosphorylated mutant, serines in SR and SP dipeptides (indicated in magenta) were replaced by alanines.

F Replacement of endogenous SRSF9 with FLAG-SRSF9-WT and the mutant (FLAG-SRSF9-mut). HeLa cells were transfected with control or SRSF9 siRNA (siControl or siSRSF9) in combination with an expression plasmid of siRNA-resistant FLAG-SRSF9-WT or FLAG-SRSF9-mut, cultured for 48 hours and analyzed by western

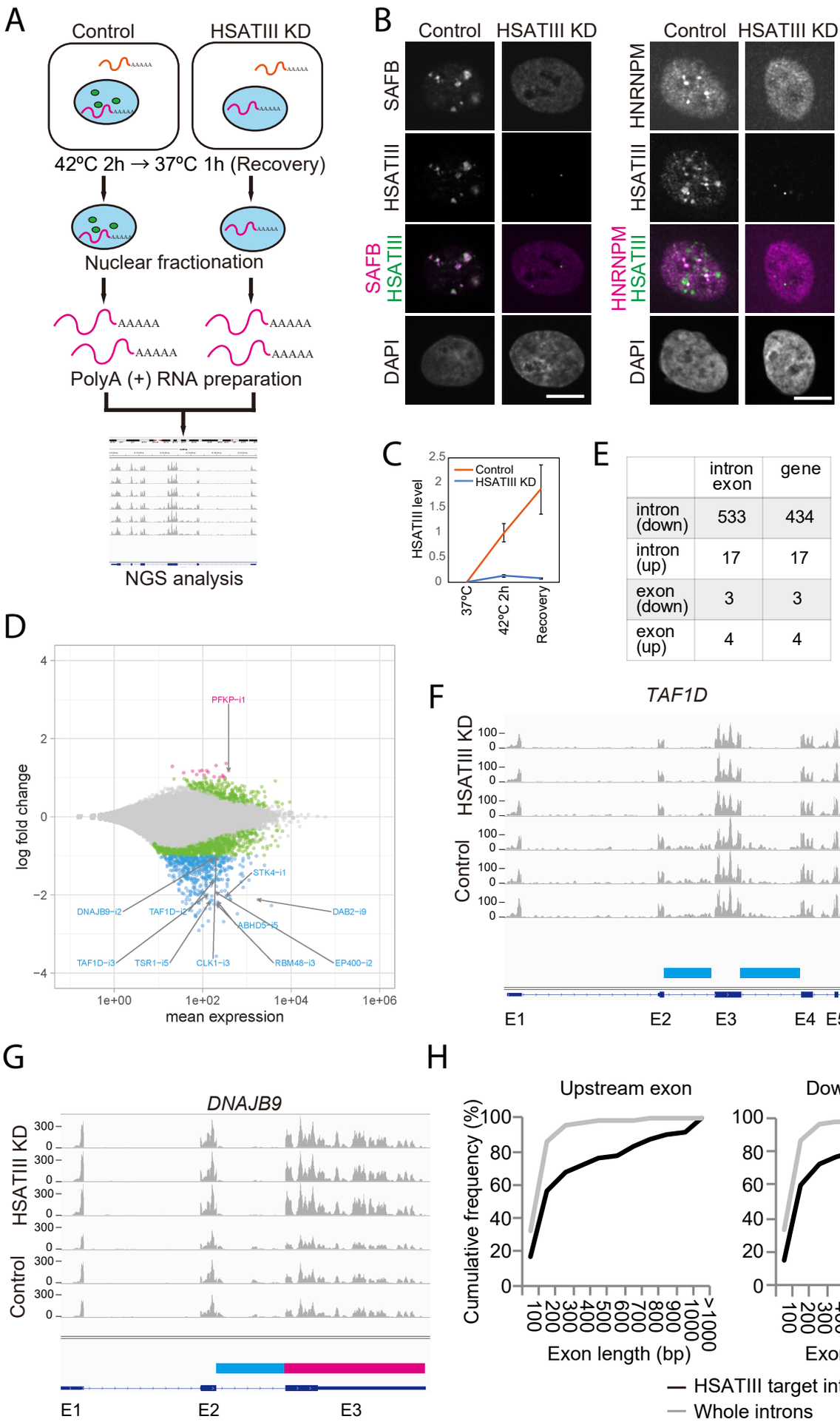
blotting. The empty plasmid was used as negative control (empty). Arrowheads and an arrow indicate exogenous and endogenous SRSF9, respectively.

G Frequency of the SRSF9 eCLIP tag on HSATIII-upregulated introns and adjacent exons. High and low coverage introns in the transcriptome samples (n=3) in Figure 1B are used as matched controls.

Table 1 Functional enrichment of HSATIII-interacting proteins

GO ID	Term	Count	P-value	Fold Enrichment	FDR
GO:0000398	mRNA splicing, via spliceosome	53	3.04E-63	29.05	4.53E-60
GO:0006397	mRNA processing	33	2.90E-34	22.43	4.32E-31
GO:0008380	RNA splicing	30	9.60E-31	21.99	1.43E-27
GO:0031124	mRNA 3'-end processing	21	1.54E-29	51.11	2.29E-26
GO:0006369	termination of RNA polymerase II transcription	22	8.55E-29	41.83	1.27E-25
GO:0006406	mRNA export from nucleus	23	8.30E-26	27.99	1.24E-22
GO:0006405	RNA export from nucleus	19	8.91E-25	42.04	1.33E-21
GO:0048025	negative regulation of mRNA splicing, via spliceosome	13	1.46E-20	75.33	2.18E-17
GO:0010467	gene expression	15	1.10E-18	38.03	1.64E-15
GO:0006376	mRNA splice site selection	10	2.81E-15	71.58	4.13E-12
GO:0000381	regulation of alternative mRNA splicing, via spliceosome	12	7.06E-15	38.43	1.06E-11
GO:0010501	RNA secondary structure unwinding	10	6.84E-11	27.65	1.02E-07
GO:0006396	RNA processing	11	6.46E-09	13.80	9.62E-06
GO:0000380	alternative mRNA splicing, via spliceosome	6	6.34E-08	52.15	9.44E-05
GO:0048026	positive regulation of mRNA splicing, via spliceosome	6	9.45E-08	48.67	1.41E-04
GO:0000375	RNA splicing, via transesterification reactions	6	1.57E-06	29.20	0.0023
GO:0045727	positive regulation of translation	7	4.43E-06	16.07	0.0066

Figure 1



	intron exon	gene
intron (down)	533	434
intron (up)	17	17
exon (down)	3	3
exon (up)	4	4

Figure 2

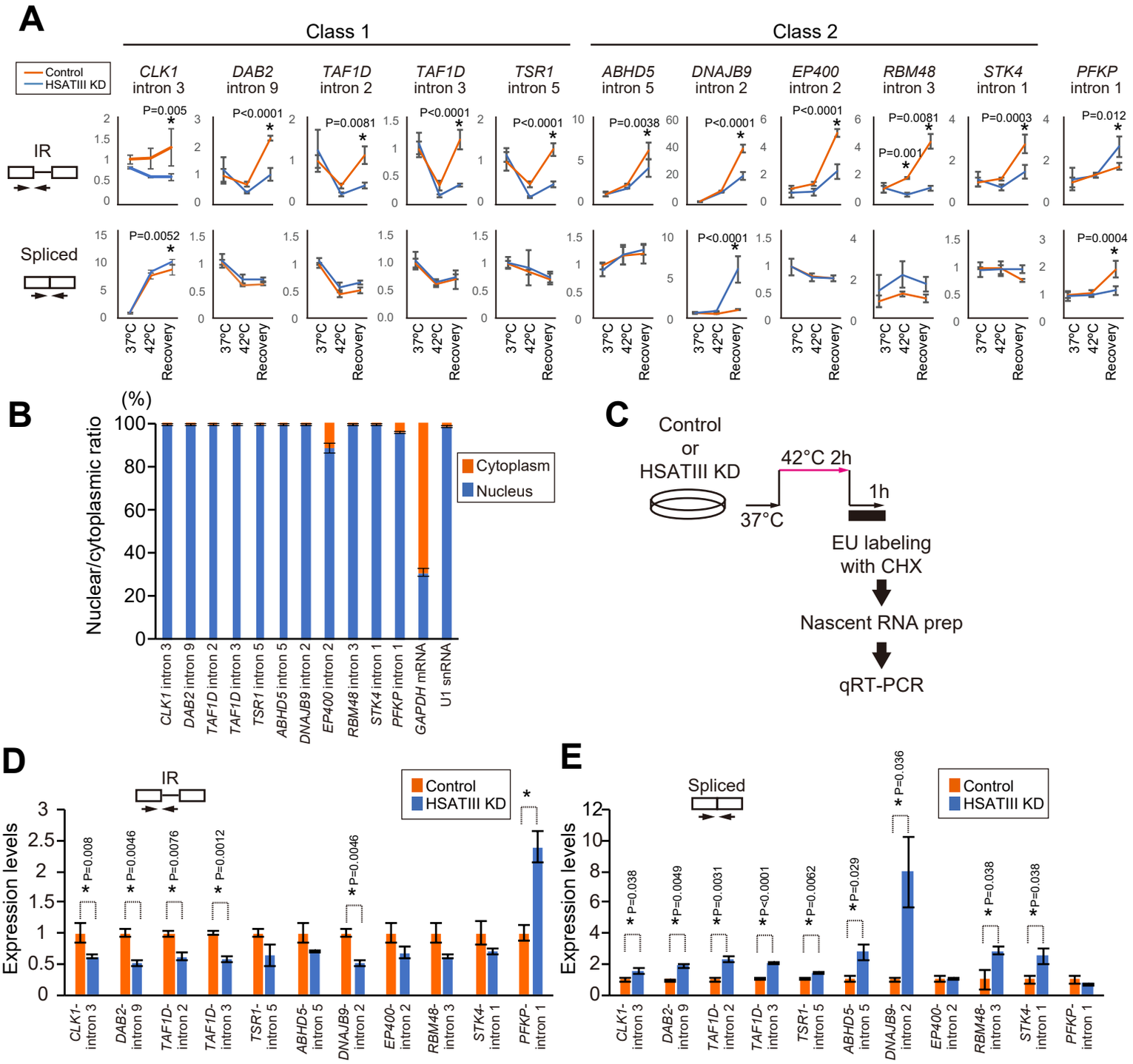

A
Class 1
Class 2
Control
HSATIII KD
CLK1 intron 3
DAB2 intron 9
TAF1D intron 2
TAF1D intron 3
TSR1 intron 5
ABHD5 intron 5
DNAJB9 intron 2
EP400 intron 2
RBM48 intron 3
STK4 intron 1
PFKP intron 1
IR
Spliced
P=0.005
P<0.0001
P=0.0081
P<0.0001
P<0.0001
P=0.0038
P<0.0001
P<0.0001
P=0.0081
P=0.001
P=0.0003
P=0.012
P=0.0052
P<0.0001
P=0.0004
37°C
42°C
Recovery
B
(%)
Nuclear/cytoplasmic ratio
Cytoplasm
Nucleus
CLK1 intron 3
DAB2 intron 9
TAF1D intron 2
TAF1D intron 3
TSR1 intron 5
ABHD5 intron 5
DNAJB9 intron 2
EP400 intron 2
RBM48 intron 3
STK4 intron 1
PFKP intron 1
GAPDH mRNA
U1 snRNA
C
Control
or
HSATIII KD
42°C 2h
37°C
1h
EU labeling
with CHX
Nascent RNA prep
qRT-PCR
D
IR
Control
HSATIII KD
Expression levels
P=0.008
P=0.0046
P=0.0076
P=0.0012
P=0.0046
E
Spliced
Control
HSATIII KD
Expression levels
P=0.038
P=0.0049
P=0.0031
P<0.0001
P=0.0062
P=0.029
P=0.036
P=0.038
P=0.038

Figure 3

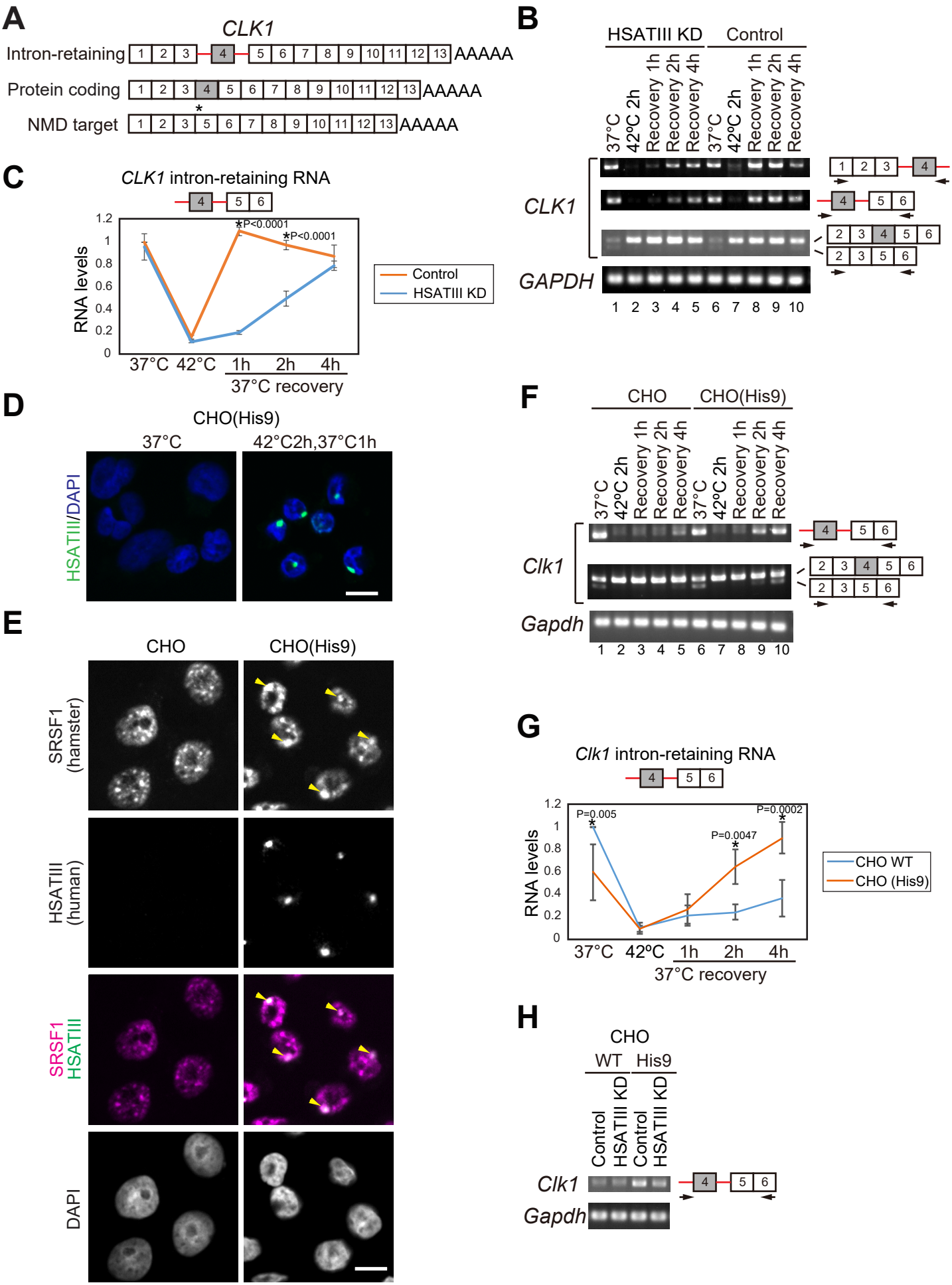

A
CLK1
Intron-retaining
Protein coding
NMD target
AAAAA
B
HSATIII KD
Control
37°C
42°C 2h
Recovery 1h
Recovery 2h
Recovery 4h
CLK1
GAPDH
1 2 3 4 5 6 7 8 9 10
C
CLK1 intron-retaining RNA
RNA levels
P<0.0001
P<0.0001
37°C 42°C 1h 2h 4h
37°C recovery
Control
HSATIII KD
D
CHO(His9)
37°C
42°C2h,37°C1h
HSATIII/DAPI
E
CHO
CHO(His9)
SRSF1 (hamster)
HSATIII (human)
SRSF1 HSATIII
DAPI
F
CHO
CHO(His9)
Clk1
Gapdh
G
Clk1 intron-retaining RNA
RNA levels
P=0.005
P=0.0047
P=0.0002
37°C 42°C 1h 2h 4h
37°C recovery
CHO WT
CHO (His9)
H
CHO
WT
His9
Control
HSATIII KD
Clk1
Gapdh

Figure 4

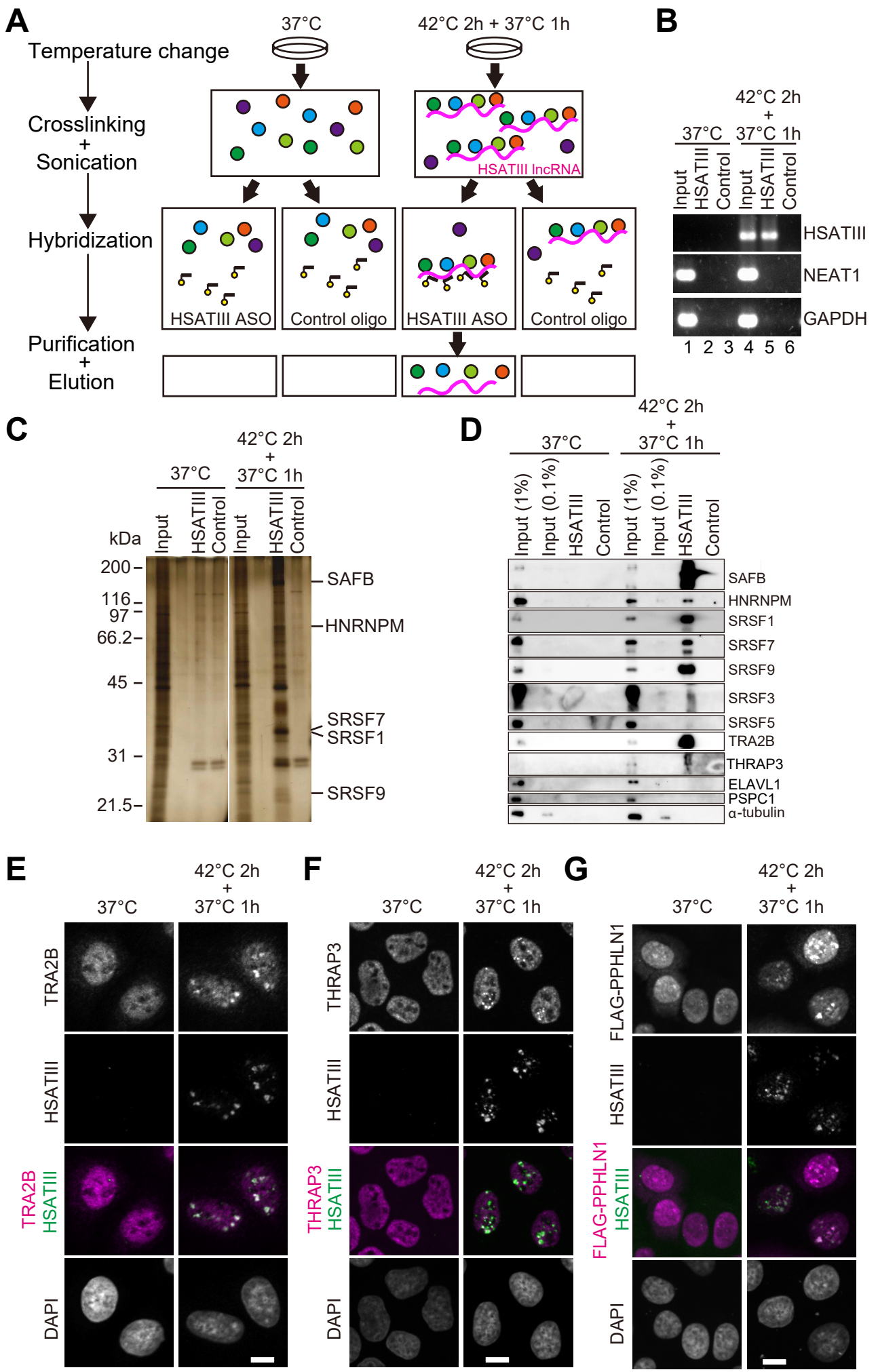

A
Temperature change
Crosslinking + Sonication
Hybridization
Purification + Elution
37°C
42°C 2h + 37°C 1h
HSATIII lncRNA
HSATIII ASO
Control oligo
HSATIII ASO
Control oligo
B
42°C 2h + 37°C 1h
37°C
Input
HSATIII
Control
HSATIII
NEAT1
GAPDH
1 2 3 4 5 6
C
kDa
200
116
97
66.2
45
31
21.5
SAFB
HNRNPM
SRSF7
SRSF1
SRSF9
D
Input (1%)
Input (0.1%)
HSATIII
Control
SAFB
HNRNPM
SRSF1
SRSF7
SRSF9
SRSF3
SRSF5
TRA2B
THRAP3
ELAVL1
PSPC1
α-tubulin
E
TRA2B
HSATIII
DAPI
F
THRAP3
HSATIII
DAPI
G
FLAG-PPHLN1
HSATIII
DAPI

Figure 5

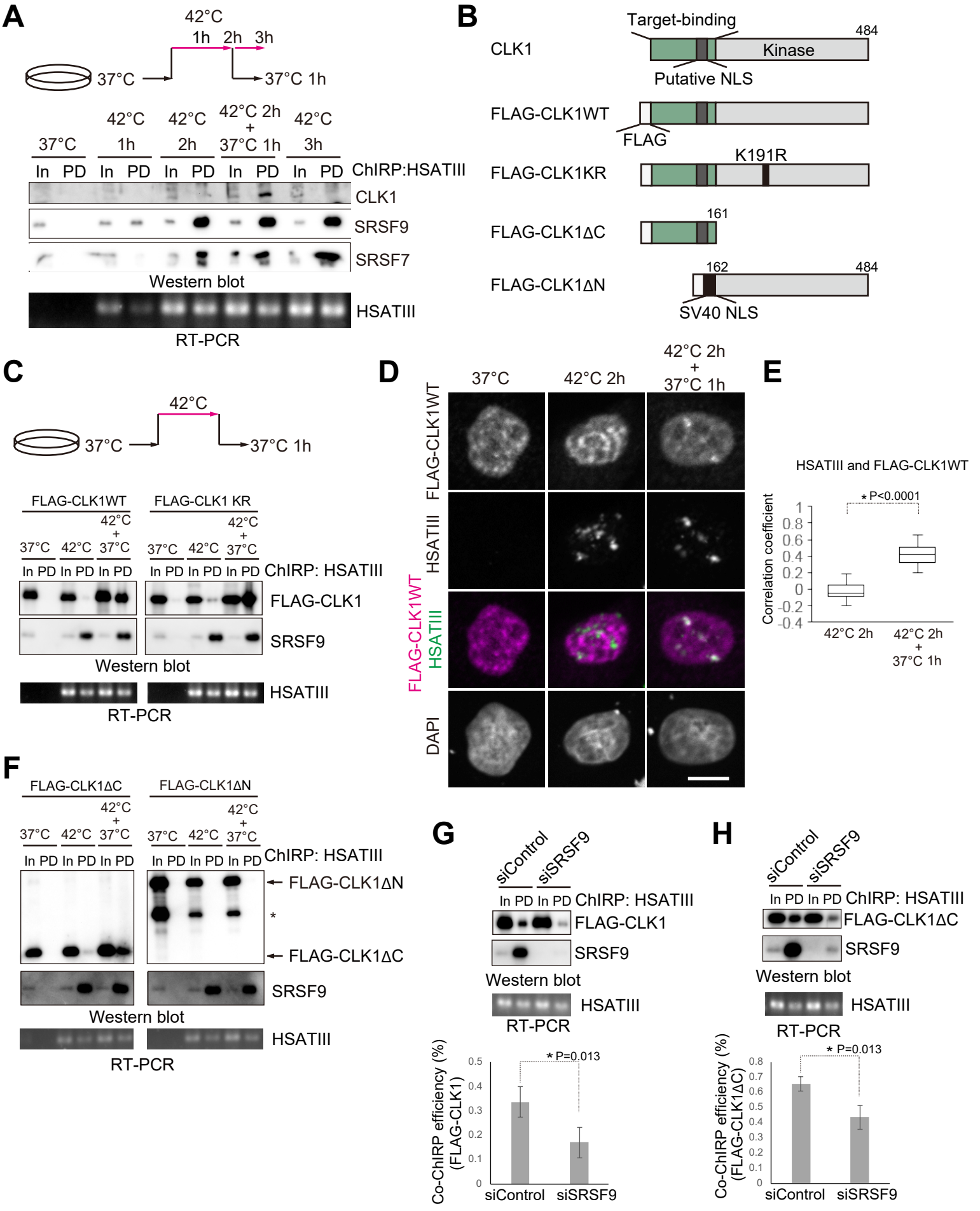

A
42°C
1h 2h 3h
37°C
37°C 1h
42°C 1h
42°C 2h
42°C 2h + 37°C 1h
42°C 3h
37°C
In PD In PD In PD In PD In PD
ChIRP:HSATIII
CLK1
SRSF9
SRSF7
Western blot
HSATIII
RT-PCR
B
CLK1
Target-binding
Kinase
Putative NLS
484
FLAG-CLK1WT
FLAG
FLAG-CLK1KR
K191R
FLAG-CLK1ΔC
161
FLAG-CLK1ΔN
162
SV40 NLS
C
42°C
37°C
37°C 1h
FLAG-CLK1WT
FLAG-CLK1 KR
42°C + 37°C
37°C 42°C 42°C + 37°C
In PD In PD In PD
ChIRP: HSATIII
FLAG-CLK1
SRSF9
Western blot
HSATIII
RT-PCR
D
37°C
42°C 2h
42°C 2h + 37°C 1h
FLAG-CLK1WT
HSATIII
FLAG-CLK1WT
HSATIII
DAPI
E
HSATIII and FLAG-CLK1WT
* P<0.0001
Correlation coefficient
1
0.8
0.6
0.4
0.2
0
-0.2
-0.4
42°C 2h
42°C 2h + 37°C 1h
F
FLAG-CLK1ΔC
FLAG-CLK1ΔN
42°C + 37°C
37°C 42°C 42°C + 37°C
In PD In PD In PD In PD In PD In PD
ChIRP: HSATIII
FLAG-CLK1ΔN
*
FLAG-CLK1ΔC
SRSF9
Western blot
HSATIII
RT-PCR
G
siControl
siSRSF9
In PD In PD
ChIRP: HSATIII
FLAG-CLK1
SRSF9
Western blot
HSATIII
RT-PCR
Co-ChIRP efficiency (%) (FLAG-CLK1)
* P=0.013
0.5
0.4
0.3
0.2
0.1
0
siControl
siSRSF9
H
siControl
siSRSF9
In PD In PD
ChIRP: HSATIII
FLAG-CLK1ΔC
SRSF9
Western blot
HSATIII
RT-PCR
Co-ChIRP efficiency (%) (FLAG-CLK1ΔC)
* P=0.013
0.8
0.7
0.6
0.5
0.4
0.3
0.2
0.1
0
siControl
siSRSF9

Figure 6

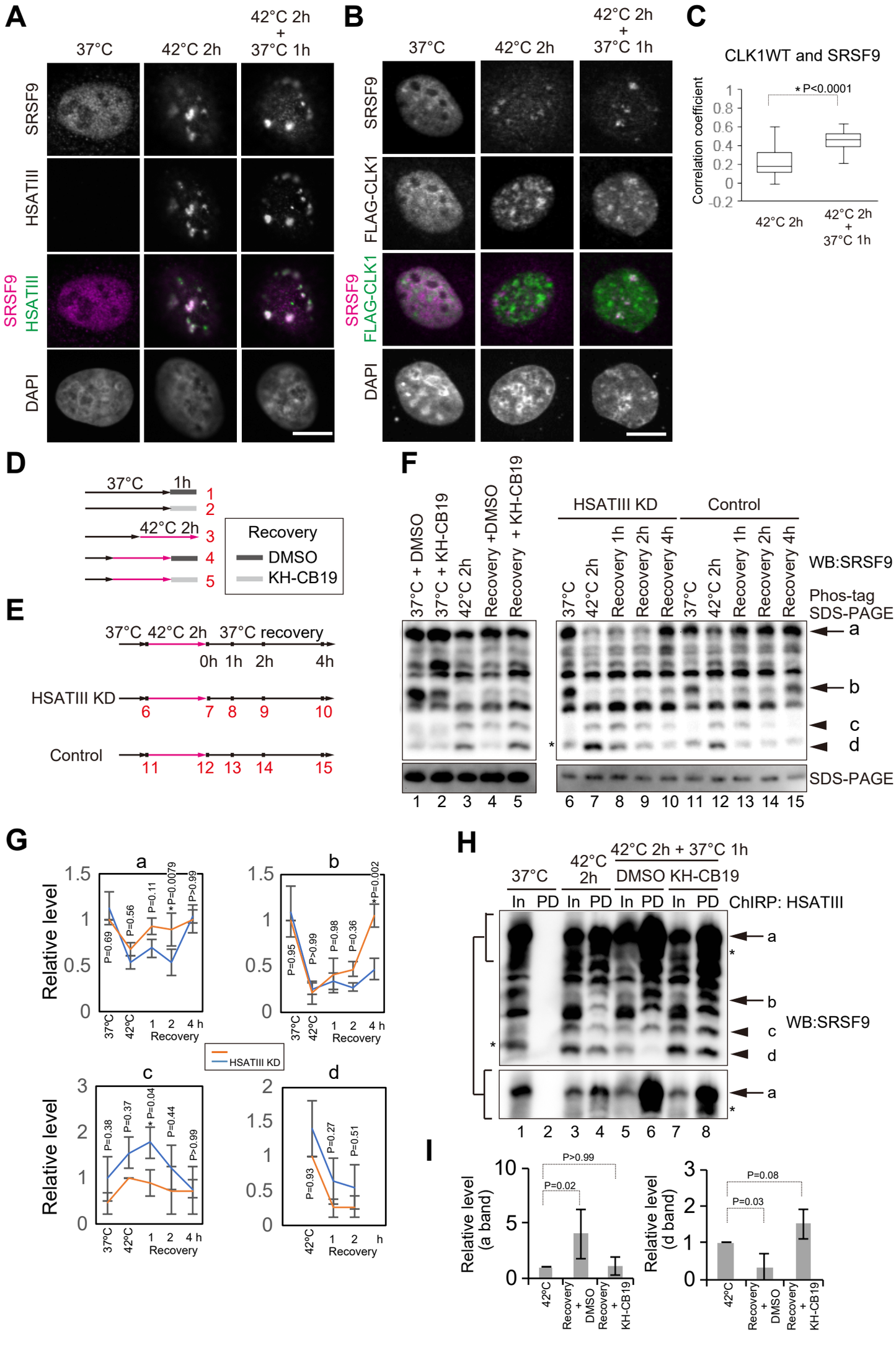

A
37°C
42°C 2h
42°C 2h + 37°C 1h
SRSF9
HSATIII
SRSF9 HSATIII
DAPI
B
37°C
42°C 2h
42°C 2h + 37°C 1h
SRSF9
FLAG-CLK1
SRSF9 FLAG-CLK1
DAPI
C
CLK1WT and SRSF9
Correlation coefficient
* P<0.0001
42°C 2h
42°C 2h + 37°C 1h
D
37°C 1h
42°C 2h
Recovery
DMSO
KH-CB19
E
37°C 42°C 2h 37°C recovery
0h 1h 2h 4h
HSATIII KD
Control
F
37°C + DMSO
37°C + KH-CB19
42°C 2h
Recovery +DMSO
Recovery + KH-CB19
HSATIII KD
Control
37°C
42°C 2h
Recovery 1h
Recovery 2h
Recovery 4h
WB:SRSF9
Phos-tag SDS-PAGE
SDS-PAGE
G
Relative level
a
b
c
d
HSATIII KD
Recovery
H
37°C
42°C 2h
42°C 2h + 37°C 1h
DMSO
KH-CB19
In PD
ChIRP: HSATIII
WB:SRSF9
I
Relative level (a band)
Relative level (d band)
P>0.99
P=0.02
P=0.08
P=0.03
42°C
Recovery + DMSO
Recovery + KH-CB19

Figure 7

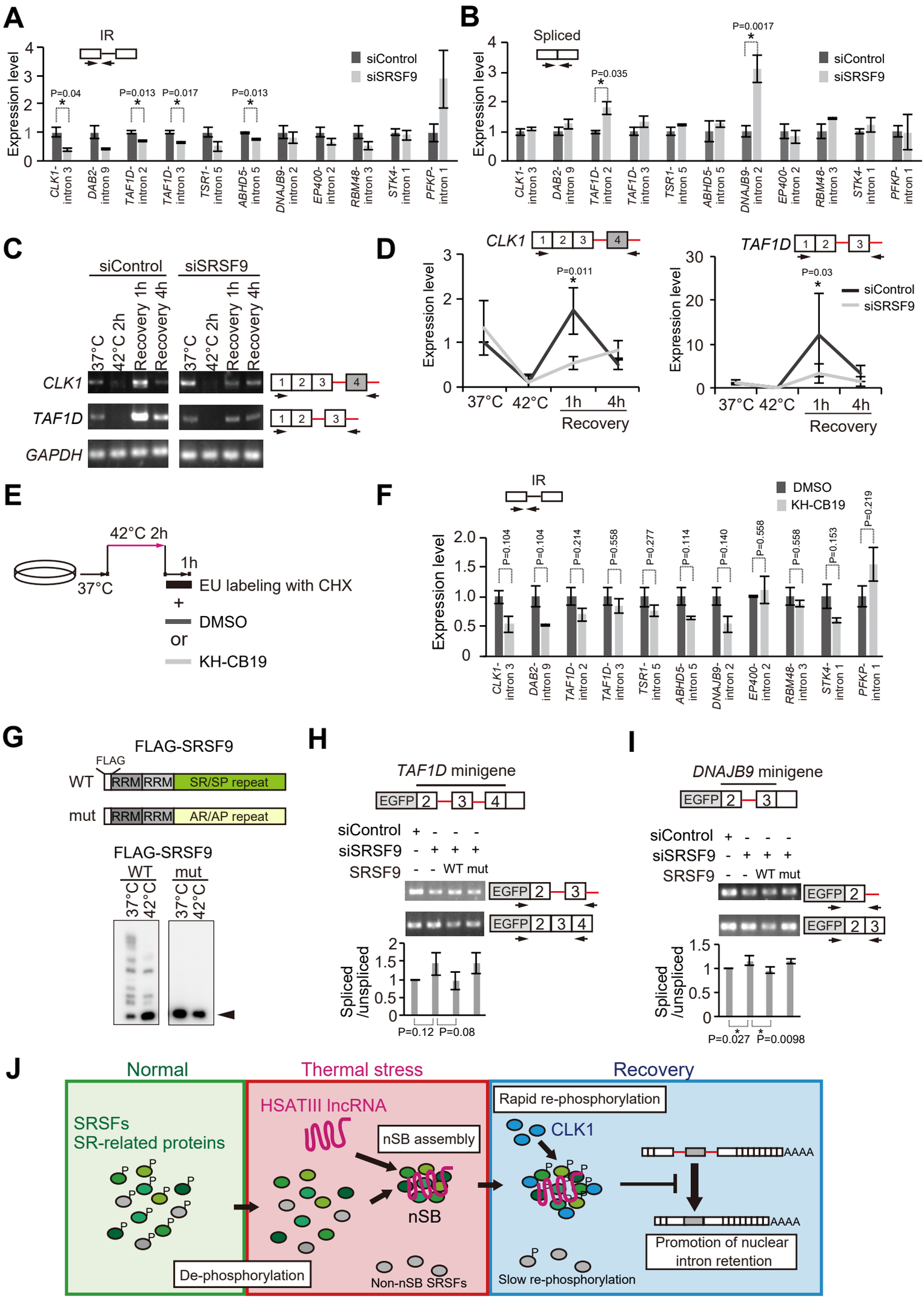
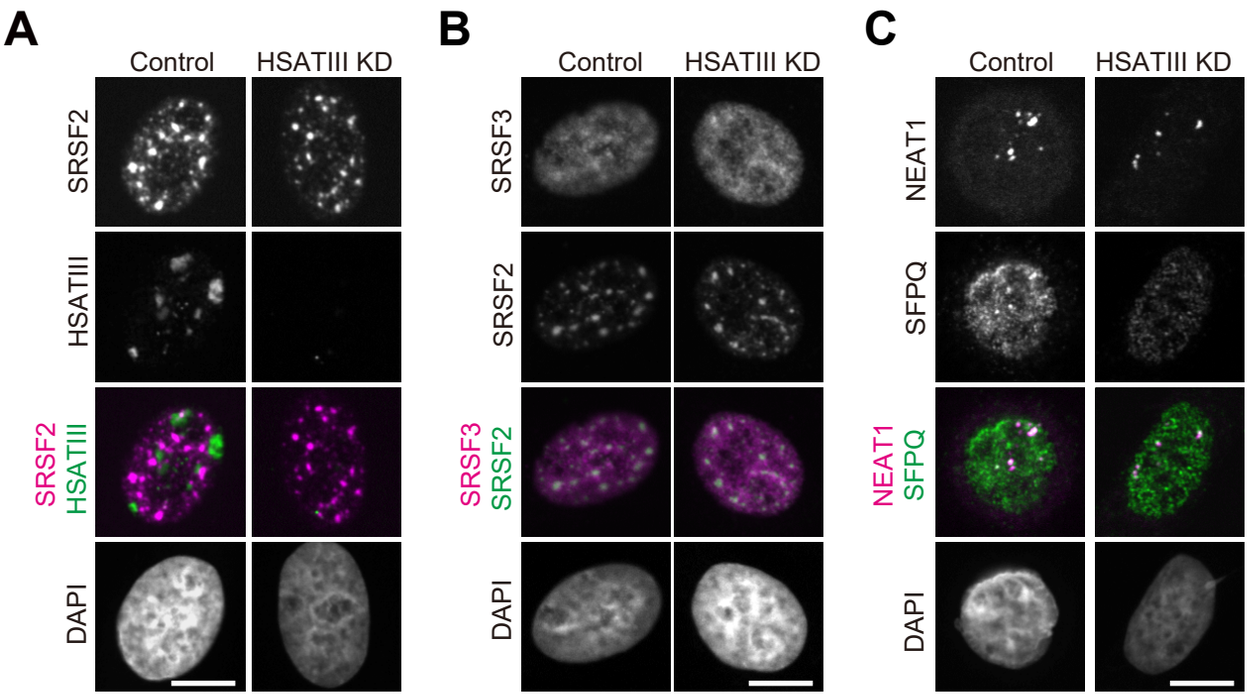
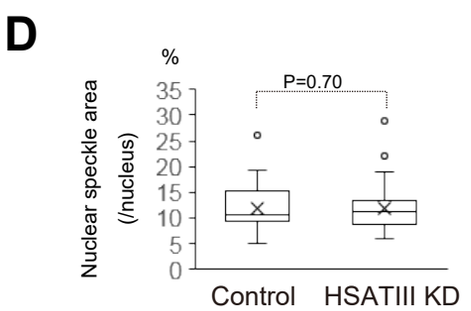
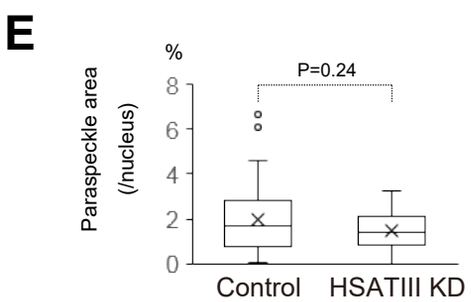

A
IR
Expression level
siControl
siSRSF9
P=0.04
P=0.013
P=0.017
P=0.013
CLK1- intron 3
DAB2- intron 9
TAF1D- intron 2
TAF1D- intron 3
TSR1- intron 5
ABHD5- intron 5
DNAJB9- intron 2
EP400- intron 2
RBM48- intron 3
STK4- intron 1
PFKP- intron 1
B
Spliced
P=0.035
P=0.0017
C
siControl
siSRSF9
37°C
42°C 2h
Recovery 1h
Recovery 4h
CLK1
TAF1D
GAPDH
D
CLK1
TAF1D
P=0.011
P=0.03
37°C 42°C 1h 4h
Recovery
E
42°C 2h
1h
37°C
EU labeling with CHX
+
DMSO
or
KH-CB19
F
DMSO
KH-CB19
P=0.104
P=0.104
P=0.214
P=0.558
P=0.277
P=0.114
P=0.140
P=0.558
P=0.558
P=0.153
P=0.219
G
FLAG-SRSF9
FLAG
WT
RRM RRM
SR/SP repeat
mut
AR/AP repeat
FLAG-SRSF9
WT
mut
37°C
42°C
H
TAF1D minigene
EGFP 2 3 4
siControl + - - -
siSRSF9 - + + +
SRSF9 - - WT mut
EGFP 2 3
EGFP 2 3 4
Spliced /unspliced
P=0.12
P=0.08
I
DNAJB9 minigene
EGFP 2 3
siControl + - - -
siSRSF9 - + + +
SRSF9 - - WT mut
EGFP 2
EGFP 2 3
Spliced /unspliced
P=0.027
P=0.0098
J
Normal
Thermal stress
Recovery
SRSFs
SR-related proteins
HSATIII lncRNA
nSB assembly
nSB
Non-nSB SRSFs
De-phosphorylation
Rapid re-phosphorylation
CLK1
AAAA
AAAA
Promotion of nuclear intron retention
Slow re-phosphorylation

Figure EV1 related to Figure 1







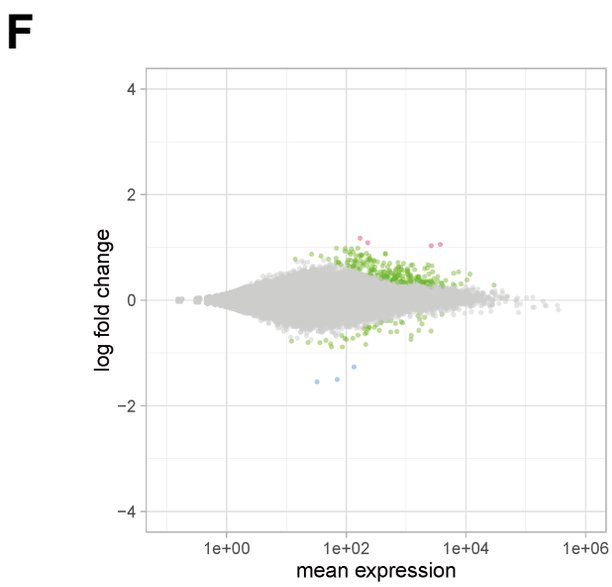


Figure EV2 related to Figure 3

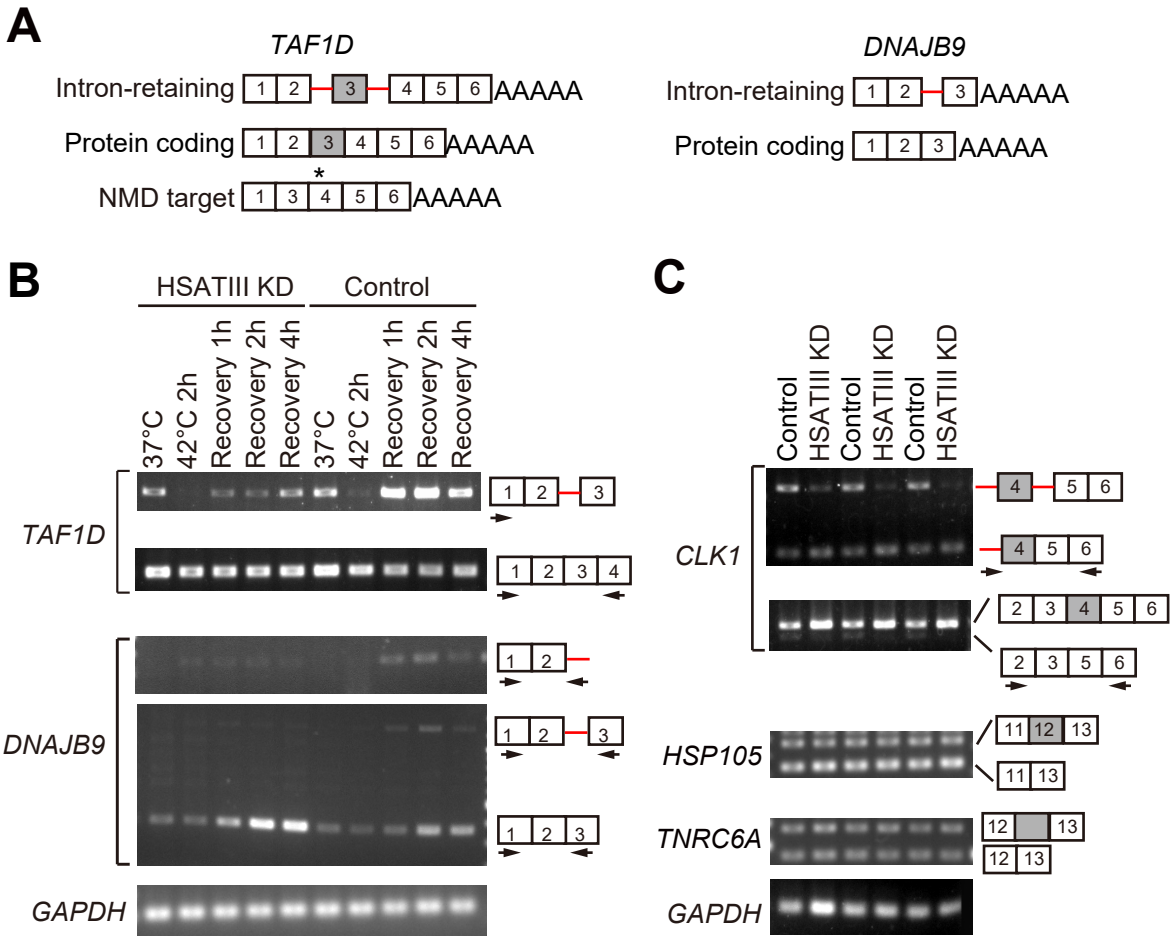


Figure EV3 related to Figure 5

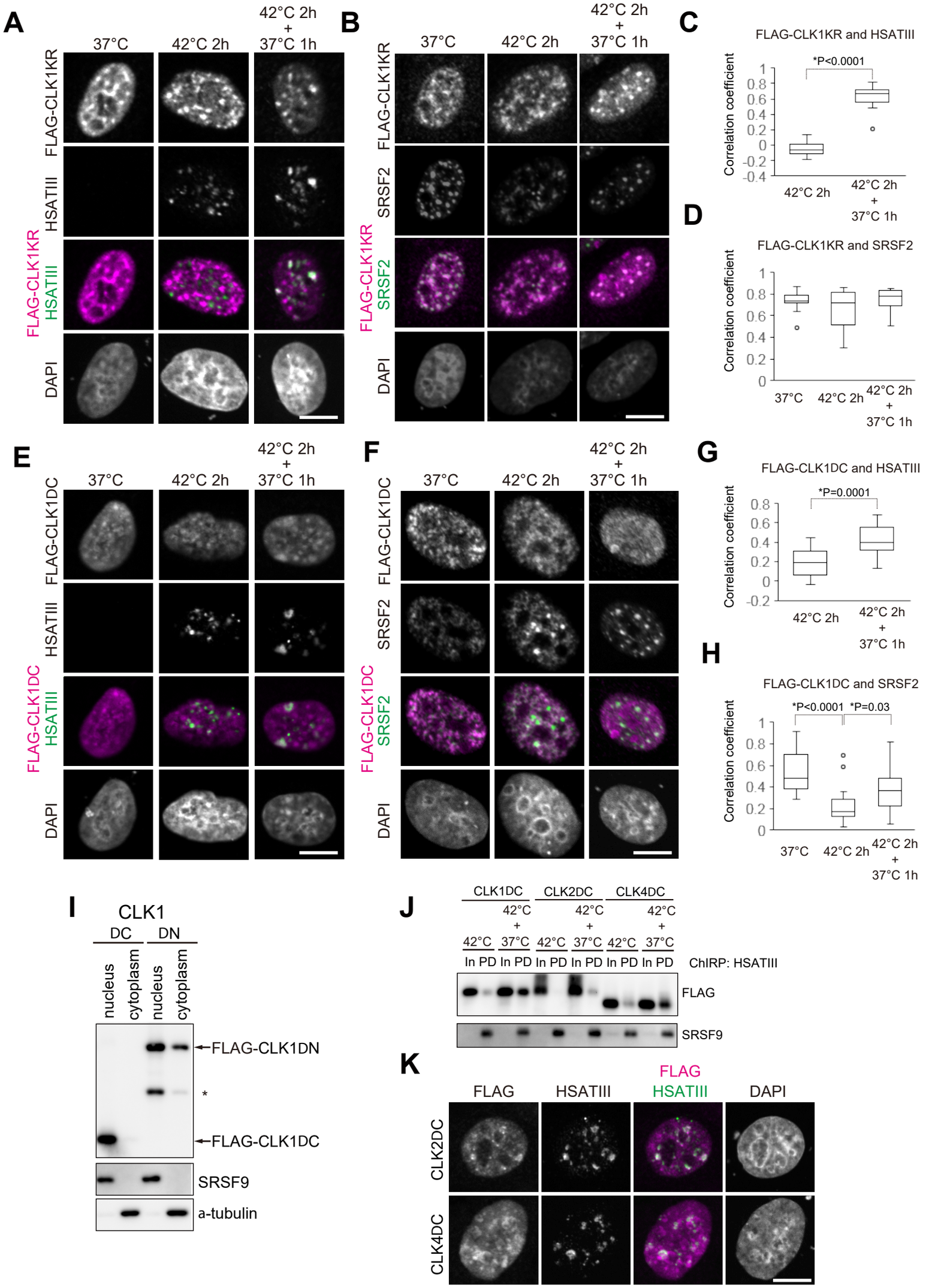


Figure EV4 related to Figure 6

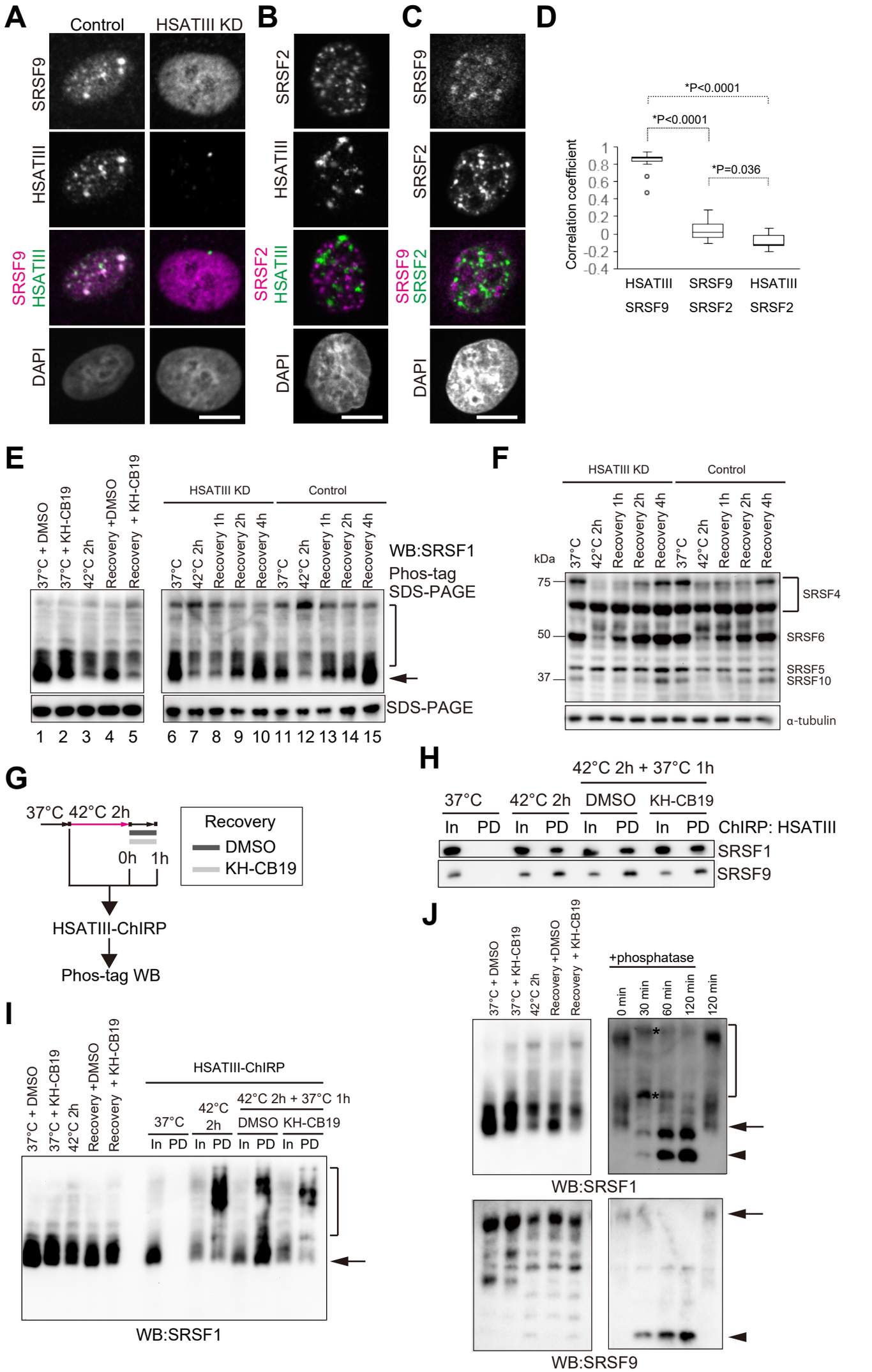
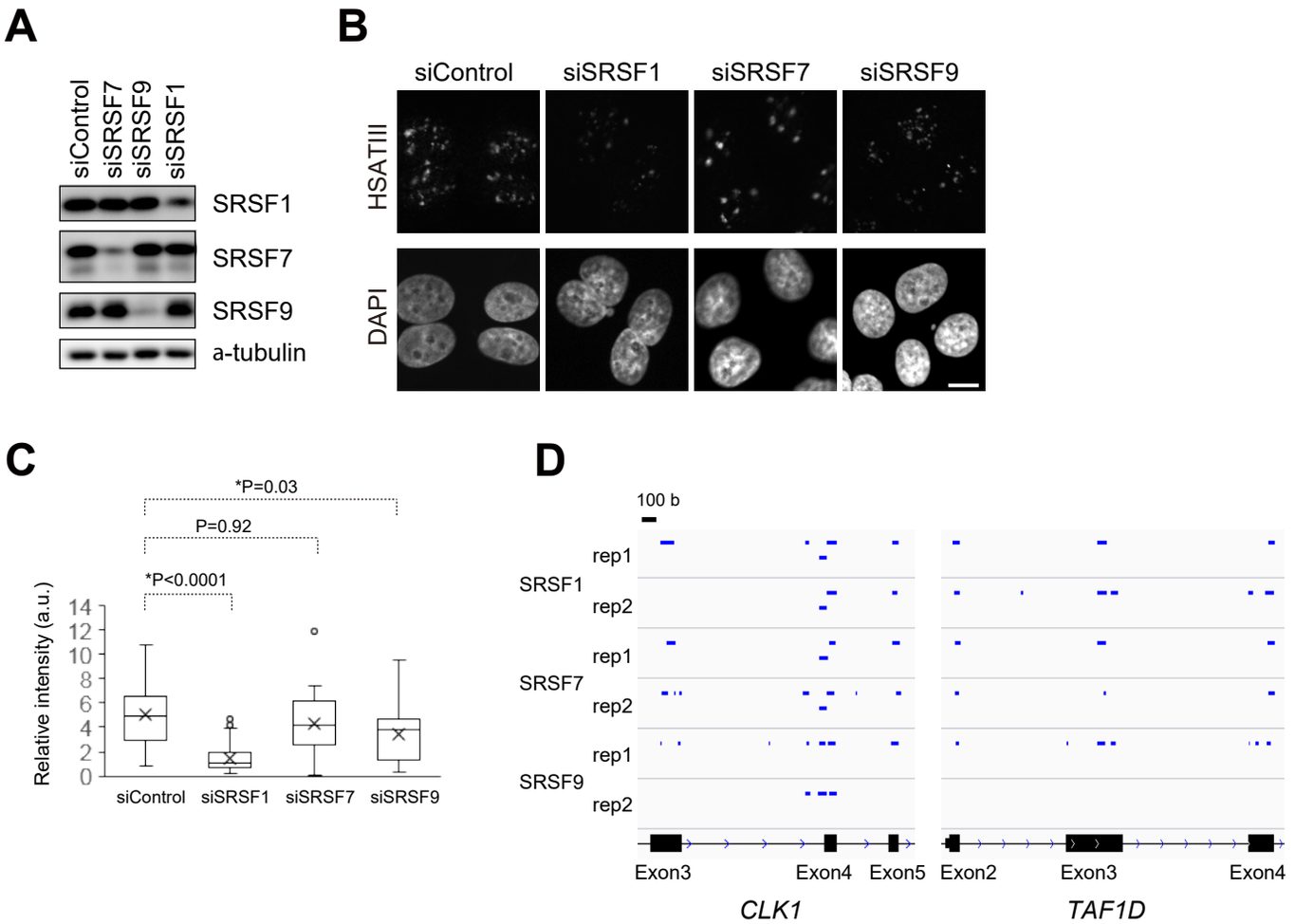
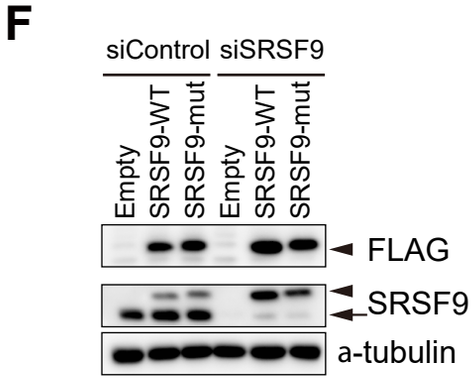


Figure EV5 related to Figure 7



E

MSGWADERGGEGDGRIYVGNLPTDVREKD
LEDLFYKYGRIREIELKNRHGLVPFAFVRFED
PRDAEDAIYGRNGYDYGQCRLRVEFPRTYG
GRGGWPRGGRNGPPTRRSDFRVLVSGLPP
SGSWQDLKDHMREAGDVCYADVQKDGVG
MVEYLRKEDMEYALRKLDDTKFRSHEGETS
YIRVYPERSTSYGYSRSRSGSRGRDSPYQS
RGSPHYFSPFRPY



G

	Upstream exon			Intron			Downstream exon		
	HSATIII-target	high coverage intron	Low coverage intron	HSATIII-target	high coverage intron	Low coverage intron	HSATIII-target	high coverage intron	Low coverage intron
Ave.lenght (b)	401.91	174.59	213.78	8685.43	1150.26	96445.33	661.22	251.44	240.47
Count rep1	397	755	353	314	895	2239	357	738	170
Count rep2	341	581	233	294	729	1938	341	541	131
Count/region rep1	0.74	0.76	0.35	0.59	0.9	2.24	0.67	0.74	0.17
Count/region rep2	0.64	0.58	0.23	0.55	0.73	1.99	0.64	0.54	0.13
Count/kb rep1	1.85	4.32	1.65	0.07	0.78	0.02	1.01	2.94	0.71
Count/kb rep2	1.59	3.33	1.09	0.06	0.63	0.02	0.97	2.15	0.54